Exploiting Aeolus Level-2B Winds to Better Characterize Atmospheric Motion Vector Bias and Uncertainty

Katherine E. Lukens[1,2], Kayo Ide[3], Kevin Garrett[1], Hui Liu[1,2], David Santek[4], Brett Hoover[4], and Ross N. Hoffman[1,2]

[1]NOAA/NESDIS/Center for Satellite Applications and Research (STAR), College Park, Maryland, 20740, USA

[2]Cooperative Institute for Satellite Earth System Studies (CISESS), University of Maryland, College Park, Maryland, 20740, USA

[3]University of Maryland, College Park, Maryland, 20740, USA

[4]Cooperative Institute for Meteorological Satellite Studies (CIMSS), University of Wisconsin-Madison, Madison, Wisconsin, 53706, USA

Correspondence to: Katherine E. Lukens (katherine.lukens@noaa.gov)

Abstract. The need for highly accurate atmospheric wind observations is a high priority in the science community, ~~and in particular~~particularly for numerical weather prediction (NWP). To address this ~~requirement~~need, this study leverages Aeolus wind LIDAR Level-2B data provided by the European Space Agency (ESA) as a potential comparison standard to better characterize atmospheric motion vector (AMV) bias and uncertainty~~, with the eventual goal of potentially improving AMV algorithms.~~. AMV products from geostationary (GEO) and low~~-~~ Earth~~ polar~~ orbiting (LEO) satellites are compared with reprocessed Aeolus horizontal line-of-sight (HLOS) global winds observed in August~~ and~~ September 2019. Winds from two ~~of the four~~ Aeolus observing modes are ~~utilized for comparison~~compared with AMVs: Rayleigh-clear (RAY) (derived from the molecular scattering signal) and Mie-cloudy (MIE) (derived from the particle scattering~~). For the most direct comparison, quality~~ signal). Quality controlled (QC'd) Aeolus winds are collocated with ~~quality controlled~~QC'd AMVs in space and time, and the AMVs are projected onto the Aeolus HLOS direction. Mean collocation differences (MCD) and the standard deviation (SD) of those differences (SDCD) are determined ~~from comparisons based on a number of conditions, and their relation to known AMV bias and uncertainty estimates is discussed. GOES-16 and LEO AMV characterizations based on Aeolus winds are described in more detail~~and analyzed.

~~Overall, QC'd AMVs correspond well with QC'd Aeolus HLOS~~ As shown in other comparison studies, the level of agreement between AMV and Aeolus wind velocities (HLOSV) varies with the AMV type, geographic region, and height of the collocated winds, as well as with the Aeolus observing mode. In terms of global statistics, QC'd AMVs and QC'd Aeolus HLOSV are highly correlated for both ~~Rayleigh-clear and Mie-cloudy~~ observing modes~~, despite remaining~~. Aeolus MIE winds are shown to have great potential value as a comparison standard to characterize AMVs, as MIE collocations generally exhibit

Style Definition: Normal: Space Before: 6 pt
Style Definition: Affiliation
Style Definition: Equation
Style Definition: Correspondence
Style Definition: BodyText
Style Definition: Title
Formatted: Space Before: 6 pt, Add space between paragraphs of the same style
Commented [KL1]: R2 specific point 2
Commented [KL2]: R2 specific point 1

smaller biases ~~in Aeolus winds after reprocessing. Comparisons~~ and uncertainties compared to RAY collocations. Aeolus RAY winds contribute a substantial fraction of the total SDCD in the presence of clouds where collocation/representativeness errors are also large. Stratified comparisons with Aeolus HLOSV are consistent with known AMV bias and uncertainty in the tropics, NH extratropics, ~~and in~~ the Arctic, and at mid- to upper-levels in ~~both~~ clear and cloudy scenes~~.~~ . AMVs in the SH ~~comparisons~~/Antarctic generally exhibit larger than expected MCD and SDCD~~, which could be attributed~~ most probably due to larger AMV height assignment errors ~~in regions~~and collocation/representativeness errors in the presence of high ~~winds~~wind speeds and ~~enhanced~~strong vertical wind shear~~. GOES-16 water vapor clear-sky AMVs perform best relative to Rayleigh-clear winds, with small MCD (-0.6 m s^{-1} to 0.1 m s^{-1}) and SDCD (5.4-5.6 m s^{-1}) in the NH and tropics that fall within the accepted range of AMV error values relative to radiosonde winds. Compared to Mie-cloudy winds, AMVs exhibit similar MCD and smaller SDCD (~4.4-4.8 m s^{-1}) throughout the troposphere. In polar regions, Mie-cloudy~~, particularly for RAY comparisons ~~have smaller SDCD (5.2 m s^{-1} in the Arctic, 6.7 m s^{-1} in the Antarctic) relative to Rayleigh-clear comparisons, which are larger by 1-2 m s^{-1}~~.

~~The level of agreement between AMVs and Aeolus winds varies per combination of conditions including the Aeolus observing mode coupled with AMV derivation method, geographic region, and height of the collocated winds. It is advised that these stratifications be considered in future comparison studies and impact assessments involving 3D winds. Additional bias corrections to the Aeolus dataset are anticipated to further refine the results.~~

Commented [KL3]: R2 specific point 1

1 Introduction

Formatted: Space Before: 12 pt

~~The need to improve~~Improving atmospheric 3D wind observations in the troposphere has long been a high priority in the science community. In 2018, the National Academies Press published the 2017-2027 decadal survey for Earth science and applications from space (National Academies, 2018~~), which includes~~) that included 3D winds in a series of observation requirement priorities and accompanying recommendations. The survey ~~recommends~~found that radiometry-based atmospheric motion vector (AMV) tracking should be ~~able~~an important approach to address the priority requirement of 3D winds.

AMVs are wind observations derived from tracking clouds and water vapor features in satellite images through time. Both geostationary (GEO) and polar-orbiting, i.e., low~~-earth~~ Earth orbiting (LEO), satellites observe the motion of such features in several spectral regions. ~~-~~Infrared bands that are specifically sensitive to water vapor (WV) absorption can capture different atmospheric ~~motion in two ways: motions using the same channel by tracking~~ (1) ~~water vapor cloud-top (WVcloud) channels are used to track~~ upper-level cloud ~~top motions~~ tops, and (2) water vapor motions in clear~~-sky (WVclear) channels are used~~ air related to ~~detect~~ upper-tropospheric features (~~e.g.,~~including the jet stream and atmospheric waves) ~~by tracking water vapor motions in clear air~~ (Velden et al., 1997). Window channel Infrared ~~window~~ (hereafter IR) cloud-~~track~~tracked AMVs are based on longwave and shortwave channels that are useful for detecting motions

Formatted: Font color: Auto

Formatted: Font color: Auto

Commented [KL4]: R2 specific point 3

Formatted: Font color: Auto

Formatted: Font color: Auto

Formatted: Font color: Auto

Formatted: Font color: Auto

Formatted: Font color: Auto

Formatted: Font color: Auto

Formatted: Font color: Auto

Formatted: Font color: Auto

Formatted: Font color: Auto

Formatted: Font color: Auto

Formatted: Font color: Auto

Formatted: Font color: Auto

Commented [KL5]: R1 point 2a

Formatted: Font color: Auto

Formatted: Font color: Auto

in cloudy scenes at mid- to upper-levels ~~(~~related to, e.g., cirrus clouds~~)~~, and at lower levels ~~(~~related to, e.g., low stratus clouds and fog~~)~~, respectively (Velden et al., 2005).

AMVs are regularly assimilated in numerical weather prediction (NWP), and they have been shown to positively impact operational forecast skill (e.g., Le Marshall et al., 2008; Berger et al., 2011; Wu et al., 2014). Since NWP data assimilation (DA) methods assume knowledge of observational error statistics, any improved characterization of AMV observation errors has the potential to improve NWP DA and hence forecast skill.

~~Until recently, AMVs were one of a few sources of vertically varying 2D wind observations.~~ Aeolus is a novel polar-orbiting satellite that was launched in 2018 by the European Space Agency (ESA) to observe vertical wind profiles from space (Stoffelen et al., 2005; ESA, 2008; Straume-Lindner, 2018). Onboard Aeolus is a Doppler Wind Lidar (DWL) instrument (Reitebuch et al., 2009) which observes winds ~~converted from backscatter retrievals~~ along the line-of-sight (LOS) of the DWL laser detected by precision timing of the backscattered signal. Rayleigh and Mie receivers detect molecular backscattering and aerosol and cloud backscattering, respectively (Straume et al., 2018) and are converted into horizontal LOS (HLOS) wind velocities (HLOSV). Rayleigh and Mie receivers observe both clear and cloudy scenes; hence, the resultant wind retrievals fall into one of four possible observing modes: Rayleigh-clear, Rayleigh-cloudy, Mie-clear, and Mie-cloudy. Rayleigh-clear and Mie-cloudy winds are of better quality and are recommended for use in analysis based on NWP assessments by ESA and ECMWF (Rennie and Isaksen, 2019; Rennie et al., 2020). Rayleigh-cloudy winds are not typically used as they sample the same locations as Mie-cloudy winds and are generally contaminated by the Mie channel. Mie-clear winds are routinely discarded as they are of poorer quality since the Mie backscattered signal is dominated by noise in clear conditions (Rennie et al., 2020; Abdalla et al., 2020).

This study aims to leverage Aeolus Level-2B (L2B) HLOS wind profiles as a ~~standard for~~potential comparison standard to characterize AMV observation bias and uncertainty~~, with the eventual goal of potentially improving AMV algorithms and the impact of AMV observations on NWP skill.~~. The availability of the consistent, global Aeolus dataset provides the unique opportunity to ~~directly~~ assess the performance of AMVs ~~derived from different retrieval channels~~ relative to a global reference wind profile dataset observed by a single unit. Such a direct global comparison has not previously been possible due to the ~~sparse~~limited spatial coverage of other available reference datasets, e.g., rawinsonde winds~~.~~, which are mostly available in the Northern Hemisphere over land (e.g., Chen et al., 2021; Liu~~, B.~~ et al., 2021; Martin et al., 2021). Further, Aeolus observations are made at a set of fixed vertical levels that represent the averages of accumulated measurements within vertical range bins. The thickness of these range bins increases with height to mitigate the decrease in signal strength with height (Rennie and Isaksen, 2020a). As such, height-related HLOS wind errors should be small relative to errors in AMV height assignment.

The structure of the paper is as follows: Section 2 describes the datasets used. Section 3 defines the quality controls, collocation methodology, and skill metrics. Section 4 ~~assesses the overall performance of~~compares AMVs with ~~respect to~~ collocated Aeolus RAY and MIE wind observations~~,~~ and discusses the resulting characterization of ~~AMV~~ AMVs in terms of mean

Formatted: Font color: Auto

Formatted: Font color: Auto

Formatted: Font color: Auto

Commented [KL6]: R1 point 3

collocation difference (MCD) and the standard deviation (SD) of collocation differences (SDCD) based on different sets of conditions. AMV performance metrics specific to GOES-16 and the suite of available LEO satellites are described in more detail. Section 5 summarizes the findings.

2 Data

Formatted: Space Before: 12 pt

2.1 Aeolus Level-2B winds

Formatted: Space Before: 6 pt

Aeolus Level-2B wind profiles (de Kloe, 2019; de Kloe et al., 2020) used in this study are derived from retrievals from the satellite's backup laser, known as Flight Model-B (FM-B), that was switched on in 2019. The L2B wind product consists of geo-located vector wind profiles projected along the HLOS of the FM-B laser, which points away from the sun (i.e., perpendicular to the spacecraft track) at 35° off nadir. Aeolus observations are collected as a line of profiles to the right of the satellite track. Because of the terminator orbit and sensor geometry away from the poles, winds in ascending orbits (southeast to northwest directionground track) are observed around sunset (local equator crossing time (LT) is 18:00 UTCLT), and winds in descending orbits (northeast to southwest directionground track) are observed around sunrise (local equator crossing time is 06:00 UTCLT). The satellite completes one orbit around Earth in approximately 92 minutes, and has a 7 days is theday repeat cycle.

Formatted: Font: Times New Roman

Commented [KL7]: R2 specific point 4

This study uses Aeolus wind profiles (baseline B10 product) during the period of 2 August – 16 September 2019., with 12 hours of 3 September omitted to account for the corresponding Aeolus blocklisted period (defined as a period of time when the Aeolus dataset is known to be degraded and should not be included in research or operations). The selected period of study was recommended by ESA for analysis as the Aeolus data are more stable and biases are relatively small (Rennie and Isaksen, 2019; Rennie and Isaksen, 2020a). The Aeolus winds were reprocessed by ESA using the updated L2B processor v3.3 that includes the M1 mirror temperature bias correction that was activated on 20 April 2020 (Rennie and Isaksen, 2020a). The M1 mirror temperatures are scene-dependent and vary based on the top-of-atmosphere radiation. Specifically, the M1 mirror reflects and focuses the backscattered laser signal onto the Rayleigh and Mie receivers. Therefore, changes in the mirror shape due to thermal variations result in perceived frequency shifts of the signal. The operational M1 bias correction uses instrument temperatures as predictors and innovation departures from ECMWF backgrounds as a reference, and is shown to improve the quality of the Rayleigh and Mie signal levels, reducing the Aeolus HLOS wind bias relative to ECMWF background winds by over 80%: the global average Rayleigh-clear bias decreased to near-zero and the Mie bias decreased to -0.15 m s^{-1} (Abdalla et al., 2020; information regarding the limitations of the operational M1 correction are presented in Weiler et al., 2021). In this study, profiles of Aeolus Rayleigh-clear HLOS winds (hereafter RAY winds) and Mie-cloudy HLOS winds (hereafter MIE winds) are collocated with AMVs. The AMVs projected onto the collocated Aeolus HLOS will be referred to as AMV winds and the original AMVs will be referred to as AMV wind vectors hereafter. Data from the other observing modes (Rayleigh-cloudy and Mie-clear) are of poorer quality and quantity and are not used.

Commented [KL8]: R1 point 4c

Formatted: Font color: Auto

The Aeolus winds were reprocessed by ESA using the updated L2B processor v3.3 that includes the M1 mirror temperature bias correction that was activated on 20 April 2020 (Rennie and Isaksen, 2020a). The M1 mirror temperatures are scene-dependent and vary based on the top-of-atmosphere radiation. Since the M1 mirror reflects and focuses the backscattered laser signal onto the Rayleigh and Mie receivers, changes in the mirror shape due to thermal variations result in perceived frequency shifts of the signal. The operational M1 bias correction uses instrument temperatures as predictors and innovation departures from ECMWF backgrounds as a reference, and is shown to improve the quality of the Rayleigh and Mie wind retrievals, reducing the Aeolus HLOS wind bias relative to ECMWF background winds by over 80%: the global average Rayleigh-clear bias decreased to near-zero and the Mie bias decreased to -0.15 m s^{-1} (Abdalla et al., 2020). While the M1 bias correction is capable of considerably reducing the telescope-induced wind bias, some residual bias may remain, e.g., in cases where the top-of-atmosphere reflected radiation strongly influences the telescope temperature (Weiler et al., 2021). Additionally, residual biases may remain in part due to potential calibration issues of the Aeolus L2B winds that could in turn lead to biases between Aeolus and NWP background winds (Liu et al., 2022).

Recent studies have compared Aeolus winds with various reference wind datasets for validation (e.g., rawinsondes and NWP forecasts). For example, Martin et al. (2021) validated Aeolus HLOS winds against rawinsonde and NWP forecast equivalents for 2018-2019. They found that the estimates of global mean absolute biases and standard deviations of Aeolus based on comparisons with rawinsonde, the ECMWF Integrated Forecasting System (IFS), and the German Weather Service (DWD) forecast model reference datasets are all comparable, with bias magnitudes ranging from 1.8 to 2.3 m s^{-1} for Rayleigh and 1.3 to 1.9 m s^{-1} for Mie and standard deviations ranging from 4.1 to 4.4 m s^{-1} for Rayleigh and 1.9 to 3.0 m s^{-1} for Mie. In addition, the biases vary with latitude and season in a similar way from reference dataset to reference dataset, with the largest differences observed in the tropics and extratropics, particularly during the summer/autumn season. Similarly, Straume et al. (2020) quality assessments showed good correspondence between Aeolus L2B winds and ECMWF model winds for September 2018. Even though Aeolus exhibited random errors that exceeded the mission requirements (4.3 m s^{-1} for Rayleigh) or just met the requirements (2.1 m s^{-1} for Mie), the Aeolus winds still had a positive impact on preliminary NWP experiments. (It should be noted that the results from Martin et al. (2021) and Straume et al. (2020) characterize Aeolus winds before they were reprocessed with the significant M1 wind bias correction applied. The Aeolus bias and error estimates should improve when using the reprocessed winds.) In addition, ECMWF conducted several studies to verify the quality of Aeolus observations (e.g., Rennie and Isaksen, 2019; de Kloe et al., 2020). They found that ~~with the application of~~Aeolus provides high quality wind observations relative to ECMWF backgrounds after applying the M1 bias correction and proper quality controls (QC) (see Section 3) as well as ~~Aeolus black-listed dates taken into account,~~accounting for Aeolus ~~provides high quality wind observations relative to ECMWF background~~blocklisted dates. RAY winds minus ECMWF IFS HLOS winds have a global mean of -0.04 m s^{-1} and a standard deviation of 5.3 m s^{-1}. MIE minus IFS winds have a global mean of -0.16 m s^{-1} and a smaller standard deviation of 3.8 m s^{-1} (Abdalla et al., 2020). ~~It is noted that the ECMWF model, the Integrated Forecasting System (IFS), is used as a reference in the calculation of the reprocessed Aeolus L2B winds, and thus a model dependency is introduced~~

Formatted: Font color: Auto

Commented [KL9]: R1 point 4a

Commented [KL10]: R2 specific point 5

Formatted: Font color: Auto

~~into the dataset (Weiler et al., 2021).~~ Related NWP impact assessments show that Aeolus has a positive impact on operational global forecasts (Cress, 2020; Rennie and Isaksen, 2020b) at major NWP centers including ECMWF, the ~~German Weather Service (~~DWD~~),~~, Météo-France, and the UK Met Office. ~~Additionally, recent studies have compared Aeolus winds with various benchmark wind datasets (e.g., rawinsondes and reanalyses). For example, Santek et al. (2021) found~~It is noted that ~~when taking collocated polar rawinsonde winds as~~ the ~~truth, quality controlled~~ ECMWF IFS is used as a reference in the calculation of the reprocessed ~~RAY winds share similar observation error standard deviations (5-6 m s^{-1}) but exhibit a larger wind speed~~Aeolus L2B winds (where the M1 bias ~~of -1.1 m s^{-1} with respect to comparisons of good-quality water vapor wind retrievals from the National Aeronautics and Space Administration (NASA) Aqua satellite (bias of -0.2 m s^{-1}). In~~correction is retroactively applied), and thus a ~~similar comparison to ECMWF Reanalysis v5 (ERA5), Santek et al. (2021) also found that Aeolus and Aqua share similar smaller biases (0.02-0.17 m s^{-1}) and uncertainties (~4.5 m s^{-1}) throughout the vertical.~~model dependency is introduced into the dataset (Weiler et al., 2021).

Despite the high quality and positive impacts, limitations remain with the Aeolus L2B dataset (Abdalla et al., 2020; Weiler et al., 2021). Mie and Rayleigh random errors could be further improved, as the Mie error standard deviations average to approximately 3.5 m s^{-1} and Rayleigh error standard deviations increase from 4 m s^{-1} to over 5 m s^{-1} from July to December 2019 (Abdalla et al., 2020). Further, MIE winds exhibit a slow (fast) wind speed dependent bias for high HLOS speeds of negative (positive) sign. ~~Moreover, there is currently an ECMWF model dependency in the reprocessed Aeolus L2B wind dataset (Weiler et al., 2021).~~ Additionally, at the time of writing, issues thought to be due to instrumentation or software malfunctions have become apparent that affect the quality of the winds. One specific issue is ~~the~~a more rapid decrease in the ~~internal and~~ atmospheric return ~~signals that~~signal relative to the laser energy itself, and this is linked to slowly increasing random errors for Rayleigh-clear winds (Straume et al., 2021). Efforts at ESA are currently underway to resolve these issues.

2.2 Atmospheric motion vectors

AMVs examined in this study (Tables 1-2) are operationally used ~~in~~by the National Oceanic and Atmospheric Administration (NOAA) National Centers for Environmental Prediction (NCEP) ~~operations~~ and are archived in 6-hour satellite wind (SATWND) BUFR files centered on the analysis times 00, 06, 12, and 18 UTC. All AMVs included in the SATWND files are produced by NESDIS, JMA and EUMETSAT. AMVs derived from sequences of GEO satellite images are observed equatorward of ~60° latitude~~.~~ and are stratified by type, including IR, water vapor cloudy channel (WVcloud), and water vapor clear channel (WVclear) AMVs; visible band AMVs are not used in this study. Polar AMVs (observed at latitudes poleward of 60°) are derived from cloud-tracked IR channels in areas covered by three consecutive LEO satellite images. ~~The GEO satellites include GOES-15 and GOES-16 operated by NOAA, Meteosat-8 and Meteosat-11 (the first and fourth satellites in the Meteosat Second Generation (MSG) series at the European Organization for the Exploitation of Meteorological Satellites (EUMETSAT)), Himawari-8 managed by the Japan Meteorological Agency (JMA), and INSAT-3D from the Indian Space Research Organization (ISRO). GEO AMVs in this study are derived from IR, WVcloud, and WVclear channels from the~~

Formatted: Space Before: 6 pt

Formatted: Font color: Auto

Formatted: TBD, Font: 12 pt, Font color: Auto

Commented [KL12]: R2 specific comment 6

Commented [KL11]: Replaced this information with a table

GOES Imager onboard GOES-15, the Advanced Baseline Imager (ABI) onboard GOES-16, the Spinning Enhanced Visible and Infrared Imager (SEVIRI) onboard Meteosat-8 and Meteosat-11, the Advanced Himawari Imager (AHI) onboard Himawari-8, and the INSAT Imager onboard INSAT-3D. (It is noted that Himawari-8 and INSAT-3D WVclear AMVs are not included in the NCEP data archive.).

AMVs from LEO satellites include several operated by NOAA: NOAA-15, -18, -19, -20 and Suomi National Polar-orbiting Partnership (S-NPP). Additional LEO satellites include MetOp-A and MetOp-B operated by EUMETSAT, and Aqua and Terra operated by NASA. LEO AMVs considered for analysis are derived from cloud-track IR window channels from instruments including but not limited to: The Visible and Infrared Imaging Radiometer Suite (VIIRS) onboard NOAA-20 and S-NPP; the Advanced Very High Resolution Radiometer (AVHRR) instrument onboard NOAA-15, -18, -19, MetOp-A, and MetOp-B; and the Moderate Resolution Imaging Spectroradiometer (MODIS) onboard Aqua and Terra.

Commented [KL13]: Replaced this information with a table

Table 1: Collocation counts for each type of GEO AMV. The table lists total counts (RAY + MIE) and counts (and % of total in parentheses) of collocated AMVs with QI > 80% that pass RAY QC and MIE QC.

Satellite	*Operator*	*Sensor*	*Total Collocation Counts*			*Counts (%) Passing RAY QC*			*Counts (%) Passing MIE QC*		
			IR	WVcloud	WVclear	IR	WVcloud	WVclear	IR	WVcloud	WVclear
GOES-15	NOAA	GOES Imager	102019	26580	17509	15389 (15.1)	7089 (26.7)	6700 (38.3)	16825 (16.5)	9053 (34.1)	935 (5.3)
GOES-16	NOAA	ABI	138851	40197	34784	22723 (16.4)	11380 (28.3)	15180 (43.6)	31200 (22.5)	18418 (45.8)	1480 (4.3)
Himawari-8	JMA	AHI	84359	49892	—	20565 (24.4)	22170 (44.4)	—	24066 (28.5)	17215 (34.5)	—
INSAT 3D	ISRO	INSAT Imager	30724	20089	—	1353 (4.4)	1916 (9.5)	—	1133 (3.7)	551 (2.7)	—
Meteosat-8	EUMETSAT	SEVIRI	80966	69405	31426	11722 (14.5)	18505 (26.7)	5612 (17.9)	14070 (17.4)	20714 (29.8)	582 (1.9)
Meteosat-11	EUMETSAT	SEVIRI	75192	57975	32948	11118 (14.8)	16694 (28.8)	6047 (18.4)	11977 (15.9)	17022 (29.4)	510 (1.5)

Table 2: As in Table 1 but for all LEO IR window channel AMVs.

Satellite	*Operator*	*Sensor*	*Total Collocation Counts*	*Counts (%) Passing RAY QC*	*Counts (%) Passing MIE QC*
Aqua	NASA	MODIS	32806	1732 (5.3)	1882 (5.7)
MetOp-A	EUMETSAT	AVHRR	27710	2935 (10.6)	4930 (17.8)
MetOp-B	EUMETSAT	AVHRR	31258	3354 (10.7)	5652 (18.1)
NOAA-15	NOAA	AVHRR	4879	489 (10.0)	654 (13.4)
NOAA-18	NOAA	AVHRR	3822	358 (9.4)	557 (14.6)
NOAA-19	NOAA	AVHRR	10456	1074 (10.3)	1308 (12.5)
NOAA-20	NOAA	VIIRS	70610	5230 (7.4)	9598 (13.6)
S-NPP	NOAA	VIIRS	60395	4262 (7.1)	8268 (13.7)
Terra	NASA	MODIS	17818	1916 (10.8)	2571 (14.4)

Numerous studies have evaluated bias and uncertainty characteristics of AMVs through direct comparison with *in situ* ~~radio-/~~rawinsonde observations and NWP analyses (e.g., Velden et al., 1997; Bormann et al., 2002, 2003; Le Marshall et al., 2008; Bedka et al., 2009; Velden and Bedka, 2009; Key et al., 2016; Daniels et al., 2018; Cotton et al., 2020). The derived motion wind algorithms that generate ~~AMVs from~~ IR, WVcloud, and WVclear ~~channels~~AMVs can vary between centers (Santek et al., 2014; Santek et al., 2019). ~~Available~~ AMV performance metrics vary significantly by season, level, channel, satellite/producer, etc. (e.g., ~~are presented in Table 1~~Santek et al., 2019; Daniels et al., 2018; Cotton et al., 2020; Key et al., 2016; Le Marshall et al., 2008). For example, typical values of AMV wind speed bias acquired from seven different data producers and ~~include results~~verified against rawinsonde winds can range from ~~comparisons of all GEO AMVs~~ -1.8 m s^{-1} to 0.3 m s^{-1}, and wind speed uncertainty represented by standard deviation can range from ~~specific examples~~4 to 6.5 m s^{-1}, with higher vector wind root mean square errors of ~~GEO and LEO satellites (6-9 m s^{-1}~~. Even for a single satellite, e.g., GOES-16~~, and~~ or Aqua ~~and Terra, respectively).~~, speed bias and uncertainty can vary geographically as well as vertically.

Formatted: Font: Italic

Formatted: TBD, Font: 12 pt, Font color: Auto

Formatted: TBD, Font: 12 pt

Formatted: TBD, Font: 12 pt, Font color: Auto

Formatted: TBD, Font: 12 pt, Font color: Auto

Formatted: TBD, Font: 12 pt, Font color: Auto

Formatted: TBD, Font: 12 pt, Font color: Auto

Formatted: TBD, Font: 12 pt, Font color: Auto

Formatted: TBD, Font: 12 pt, Font color: Auto

Commented [KL14]: R2 specific comment 7

Formatted: TBD, Font: 12 pt, Font color: Auto

Formatted: Font color: Red

Table 1: Summary of published statistics of AMV performance. IR indicates the IR-window channel. NA denotes unavailable information from the sources used. Sources include [1]Santek et al. (2019) for July, AMV QI ≥ 80%; [2]Daniels et al. (2018) for November, QI ≥ 60%; [3]Cotton et al. (2020) for November, QI ≥ 80%; [4]Key et al. (2016) for March-August, No QI used; [5]Le Marshall et al. (2008) for May-January, QI ≥ 85%.

AMV Source	*Region*	*Verification*	*Speed Bias ($m s^{-1}$)*	*Speed SD, RMS ($m s^{-1}$)*	*Vector Diff ($m s^{-1}$)*	*Vector RMS ($m s^{-1}$)*
[1]All GEO	Global	Radiosonde	-1.79 to 0.31	4.07 to 6.54	NA	5.93 to 8.97
[1]All GEO	Global	NWP Analysis	-1.12 to 0.26	1.11 to 4.57	2.59 to 5.54	3.10 to 7.53
[2]GOES-16, IR	Full Disk	Radiosonde	~ -1.0 to 0.50	NA	~ 3.00 to 6.00	NA
[3]GOES-16, IR	NH, upper levels	GFS Background	-0.56	3.54	NA	NA
[3]GOES-16, IR	Tropics, upper levels	GFS Background	-0.67	3.61	NA	NA
[3]GOES-16, IR	SH, upper levels	GFS Background	-0.06	3.51	NA	NA
[4,5]AQUA and TERRA, IR	Poles, upper levels	Radiosonde	-0.80 to -0.50	NA	4.71 to 4.81	5.22 to 5.55
[4,5]AQUA and TERRA, IR	Poles, middle levels	Radiosonde	-1.01 to -0.35	NA	4.20 to 4.38	4.79 to 5.35
[4,5]AQUA and TERRA, IR	Poles, low levels	Radiosonde	-0.91 to -0.03	NA	3.58 to 3.92	4.02 to 4.82

In fact, AMVs have state-dependent errors that can vary based on wind speed and water vapor content and gradient (Posselt et al., 2019). Past reports show that AMVs tend to exhibit a slow speed bias (1-5 $m s^{-1}$) at high levels (above 400 hPa) in the extratropics and a fast speed bias (1-3 $m s^{-1}$) at middle levels (400-700 hPa) in the tropics (Bormann et al., 2002; Schmetz et al., 1993; von Bremen, 2008). Recent improvements to AMV derivation schemes, e.g., in GOES-16/17 and Himawari-8, have reduced the fast speed bias, with the residual bias largely attributed to height assignment errors (Cotton et al., 2020). Height assignments to the AMVs via satellite- and ground-based techniques (Jung et al., 2010; Salonen et al., 2015) have been shown to account for a large source of AMV uncertainty (Velden and Bedka, 2009). One factor of height assignment error is that

AMVs are generally assigned to discrete levels when instead they better correlate with atmospheric motions in layers of varying depth that depend on the vertical moisture profile (Velden et al., 2005; Velden and Bedka, 2009). Moreover, speed biases and uncertainties tend to be higher at ~~heights~~higher elevations and in ~~regions~~combination with strong wind shear (Bormann et al., 2002; Cordoba et al., 2017), and this is attributable to larger height assignment errors (hereafter the wind-shear height assignment error effect).

3 Approach and quality controls

Aeolus HLOS global wind profiles are collocated with satellite-derived AMVs. The collocation approach implemented here ~~is the same employed~~was also used by Hoffman et al. (~~2021~~2022) and follows that employed at UW-Madison/Cooperative Institute for Meteorological Satellite Studies (CIMSS) (Santek et al., ~~2021).~~ 2021). AMV collocation datasets are prepared separately for RAY and MIE winds. (A single AMV might appear in both datasets.) AMV observations are compared with Aeolus observations from the same and neighboring 6-h cycles to account for all possible collocations. An Aeolus observation is retained for comparison with an AMV if the Aeolus observation satisfies *all* the following collocation criteria:

1. Aeolus time falls within 60 minutes of the AMV time.
2. Aeolus pressure is within 0.04 $\log_{10}$(pressure) of the AMV height assignment. (Note that the log of pressures is used to account for the non-linear decrease of pressure with increasing altitude.)
3. Aeolus observation location is within 100 km horizontal great circle distance of the AMV location.

If multiple Aeolus observations satisfy these criteria for the same AMV observation, the Aeolus observation closest in distance is retained. Then, if multiple Aeolus observations still meet all collocation criteria, the observation closest in pressure to the AMV observation is kept for analysis. There is no need to consider closeness in time given the collocation criteria and the Aeolus orbit. ~~Aeolus observations are collected as a line of profiles to the right of the satellite track. Since it takes approximately 92 minutes for Aeolus to complete an orbit around Earth, all observations in any one orbit that might exist within the 100 km great circle radius around an AMV observation would occur within 30 seconds of Aeolus passing overhead. The 30-second interval is irrelevant compared to the 1-hour collocation time difference criterion. Further, the only way for Aeolus observations from two distinct orbits to be collocated with the same AMV is for the time differences of both observations relative to the AMV to be greater than 30 minutes. Therefore, we only consider the closest profile and then to select the observation from that profile closest in the vertical to the AMV.~~ After collocation, the AMV wind vector is projected onto the HLOS direction of its paired Aeolus observation.

Our choice of collocation criteria is conservative compared to those defined by the IWWG 1998 workshop (Velden and Holmlund 1998). Although the larger time and distance criteria defined by IWWG (90 vs 60 minutes and 150 vs 100 km) might retain more collocation pairs and thus a larger sample, the collocated winds would more likely have larger MCD and

Formatted: Space Before: 12 pt

Formatted: Font: Times New Roman

Formatted: Font: Times New Roman

Formatted: Font: Times New Roman

Commented [KL15]: R2 specific point 10

Formatted: Font: Times New Roman

Formatted: Indent: First line: 0", Add space between paragraphs of the same style

Commented [KL16]: R2 specific comment 9

Formatted: Font: Times New Roman

Formatted: Addition, Font: Times New Roman, 12 pt, Fon color: Auto

Formatted: Font: Times New Roman

SDCD. Our smaller time and distance criteria restrict the number of possible Aeolus matches to any one AMV and help avoid Aeolus matches from two different orbits. The IWWG height criterion is a fixed pressure difference (25 hPa) that might be too small at lower levels where pressure layers are tightly spaced in elevation but too large in the upper atmosphere where the elevation distance between pressure layers is much larger. Our height criterion is based on a $\log_{10}$ scale and accounts for the varying distances between pressure layers throughout the vertical and corresponds to pressure differences ranging from approximately 300 to 1 hPa for pressures from 1000 to 10 hPa, respectively.

Once collocated, Aeolus winds and AMVs are filtered by additional QC tests to retain pairs of ~~quality controlled (~~QC'd~~)~~ observations. (QC was implemented after collocation in order to test and compare the use of different QC criteria without having to repeat the collocation process.) Aeolus QC criteria were chosen following ESA's recommendations for the RAY and MIE observing modes, and these are consistent with those listed in Rennie and Isaksen (2020a). Specifically, RAY winds are rejected if winds are close to topography (pressure > 800 hPa), have horizontal accumulation ~~length~~lengths < 60 km, vertical accumulation ~~length~~lengths < 0.3 km, L2B uncertainty > 12 m s^{-1} at upper levels (pressure < 200 hPa), or L2B uncertainty > 8.5 m s^{-1} at lower levels (pressure > 200 hPa). L2B uncertainty refers to the Aeolus HLOS wind error estimate assigned to each wind measurement. Horizontal and vertical accumulation lengths refer to the horizontal and vertical distances over which individual measurement signals are accumulated and averaged to improve the signal-to-noise ratio. In this way, the Aeolus observations represent wind volumes and not discrete points or levels. The accumulation lengths can vary and depend on the processor settings. Similarly, MIE winds are rejected if winds are near topography (pressure > 800 hPa) or L2B uncertainty > 5 m s^{-1}~~.~~ at any level. For all AMVs, a forecast-independent quality indicator (QI) of at least 80% is used to filter and retain the high-quality data; this threshold is recommended for AMV studies and in NWP by the user community and has been shown to improve statistical agreement between AMV-producing centers (Santek et al., ~~2019).~~ 2019). No explicit outlier QC is applied and since there are no extreme outliers (seen below in Figs. 6 and 9), the QC that is applied is sufficient to eliminate them. Total collocation counts per satellite as well as the percentage of observations that pass QC for each AMV type and Aeolus mode are presented in Tables 1-2. (It is noted that Himawari-8 and INSAT 3D WVclear AMVs are not included in the NCEP data archive.)

~~As a case study, we examine in greater detail the performance of AMVs from GOES-16, a GEO satellite. GOES-16 AMVs are derived from full disk images centered at 75.2° W longitude from the onboard ABI. GOES-16 cloud-top AMVs are generally of good quality and when validated against radiosonde winds exhibit a relatively small mean difference in wind speed ranging from -1.0 m s^{-1} to +0.5 m s^{-1} and mean vector differences of 3-6 m s^{-1} that tend to increase with height (Table 1). Figure 1 presents the GOES-16/Aeolus collocation number densities (i.e., the total number of collocated observation pairs within each grid cell on a 1.25° (~140 km) resolution map) covering the period of study. QC'd GOES-16 AMVs collocated with QC'd RAY and MIE winds are shown in Fig. 1a and Fig. 1b, respectively. MIE collocations exhibit three bands of high-density winds along the intertropical convergence zone (ITCZ) and extratropical storm tracks, with few winds found between 0-30° S. A similar~~

Commented [KL17]: R1 point 1c

Formatted: Font: Times New Roman

Formatted: Font: Times New Roman

Formatted: Font: Times New Roman

Formatted: Font: Times New Roman, Font color: Auto

Formatted: Font: Times New Roman, Font color: Auto

Formatted: Font: Times New Roman, Font color: Auto

Formatted: Font: Times New Roman

Commented [KL18]: R1 point 5b

Commented [KL19]: R1 point 5a

Formatted: Font: Times New Roman

Formatted: Font: Times New Roman

Formatted: Font: Times New Roman, Font color: Auto

Formatted: Font: Times New Roman, Font color: Auto

Formatted: Font: Times New Roman, Font color: Auto

Formatted: Font: Times New Roman

Commented [KL20]: R2 specific points 8, 12

Formatted: Font: Times New Roman

Commented [KL21]: R2 specific point 11

Formatted: Font: Times New Roman

Formatted: Normal, Left, Line spacing: single

Formatted: Font: Times New Roman

but smoother version of the MIE distributions is shown for collocated RAY winds. The MIE collocation number density is greater than that for RAY, as AMV observation density tends to be higher in very cloudy or very moist scenes (Velden et al., 1997).

For the LEO perspective, we choose to examine the performance of all LEO AMVs derived from IR window channels rather than from a single satellite. Figure 2 depicts observation number densities of QC'd LEO AMVs collocated with QC'd RAY and MIE winds in the NH and SH polar regions bounded by 60° latitude: NH RAY (Fig. 2a), SH RAY (Fig. 2b), NH MIE (Fig. 2c), and SH MIE (Fig. 2d). In general, more LEO MIE collocation pairs pass QC and are retained in the analysis than for RAY winds. Collocations in the Arctic are found across the high latitudes with MIE comparisons exhibiting higher concentrations poleward of Eurasia and North America. Antarctic collocations are primarily found over the western half of the continent. In this region, water vapor features are more

Formatted: Font: Times New Roman

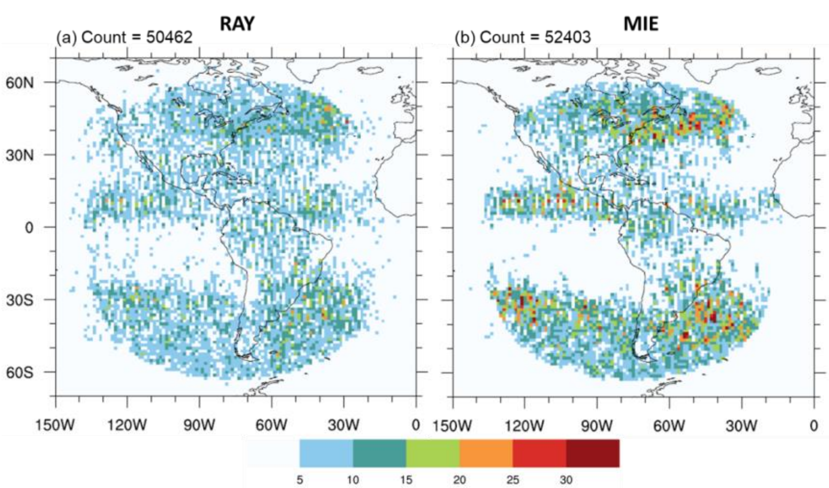

Figure 1: Number densities of quality-controlled GOES-16 AMV observations collocated with quality-controlled Aeolus (a) Rayleigh-clear (RAY), and (b) Mie-cloudy (MIE) HLOS winds. Colors indicate total number of collocated observation pairs within a grid cell at 1.25° (140 km) horizontal resolution. Total observation count per panel is displayed in the top left corner. This and all subsequent plots are for all collocations with quality controlled AMV and Aeolus winds during the study period (2 August 2019 to 16 September 2019)

suitable for tracking and deriving AMVs as they exist downstream of intense upper-level storm tracks (Hoskins and Hodges, 2005) in an area of higher annual precipitation (Grieger et al., 2015).

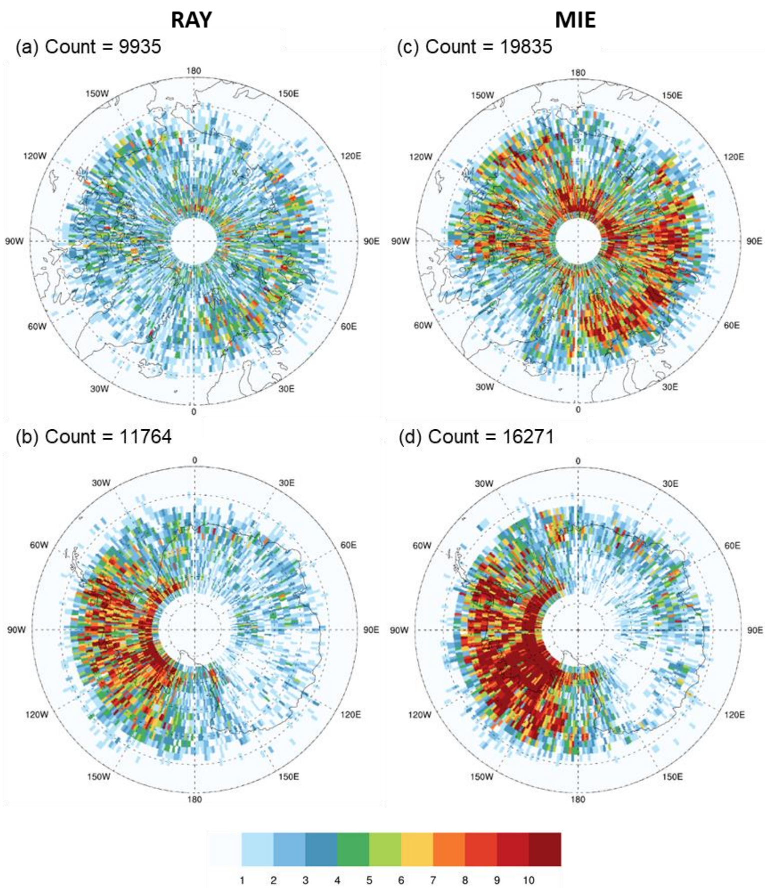

~~**Figure 2: Number densities of IR-derived AMVs from all available LEO satellites collocated with Aeolus RAY (left column) and MIE (right column) winds in the (a,c) Arctic (north of 60° N), and (b,d) Antarctic (south of 60° S). Colors indicate total number of collocated observation pairs within a grid cell at 1.25° (140 km) horizontal resolution. Dashed latitude lines are spaced every 5 degrees. Total observation count per panel is displayed in the top left corner.**~~

The performance of QC'd AMVs relative to collocated QC'd Aeolus winds ~~of QC'd~~ are characterized by analyzing the statistics of the difference AMV HLOSV minus Aeolus HLOSV. The two key statistics calculated for the collocation difference (always in the sense of AMV minus Aeolus) are the MCD and the SDCD. Because we are comparing the AMV and Aeolus HLOSV,

Formatted: Font: Times New Roman

Formatted: Font: Times New Roman

Formatted: Font: Times New Roman

Formatted: Font: Times New Roman

a scalar quantity, our statistics can only be analogs of the standard one. We include the formulae for all the statistics in Appendix A. It is important to emphasize that the collocation differences have several components that include errors in both AMVs and Aeolus winds. Specifically, these are due to the observation error of the AMVs and Aeolus HLOSV, representativeness errors due to differences in scales observed, which are related to different shapes of the observing volumes, and to collocation errors due to the space and time mismatches between the observations. As previously mentioned, the estimated SD for Aeolus L2B winds is 3.8 m s^{-1} for MIE and 5.3 m s^{-1} for RAY~~, and known AMV SD are shown in Table 1. In addition, differences due to collocation (i.e., due to different times and locations of the two observations) could play a role in increasing the differences between the collocated HLOS winds.~~. We note that it might be possible to estimate the statistics of the collocation and representativeness errors. The collocation difference may be considered to have three independent components: the error of the AMV winds, the error of the Aeolus winds, and the difference between the truth evaluated for the AMV and the Aeolus winds. We can isolate the first component, the AMV error, if we know the other two components, and we already have estimates of the second component, the Aeolus wind error in the L2B data. The last component is the error due to representativeness and collocation differences. The differences in time and location give rise to the collocation error. The difference in the shapes of the observing volumes gives rise to the representativeness error. If we simulate the AMV and Aeolus observations from a high-quality forecast or analysis or simulation, taken to be the truth, then we can calculate estimates of the combined representativeness and collocation errors. If the truth fields are simply interpolated to the observation locations then the calculated estimates are for the collocation errors alone. For this study we take the first step in isolating the collocation/representativeness errors by removing the influence of the Aeolus error from the SDCD, as the simulation of the AMV and Aeolus observations is out of the scope of this study. The removal of the Aeolus error estimate results in a smaller SDCD, which still includes AMV random and representativeness errors and collocation error. The SDCD are larger for RAY comparisons than for MIE comparisons in terms of both the original (or total) and adjusted values. Although the Aeolus L2B uncertainty is highly dependent on the time period and processor used to determine the HLOS winds, it is the correct uncertainty estimate for our study.

Commented [KL22]: R1 point 1a

Formatted: Font: Times New Roman

Commented [KL23]: R2 main point 3

Commented [KL24]: R2 main point 2

Formatted: Font: Times New Roman

The geometry of the Aeolus observation affects how the HLOS winds are interpreted for analysis (Straume et al., 2018). The observed ~~HLOS wind~~HLOSV provides both a speed and direction and represents the motion of air projected onto the line-of-sight of the laser that in 2D space is nearly orthogonal to the satellite orbit direction (see Fig. 1 in de Kloe, 2019). Thus, in the ascending orbit ~~segments~~phase away from the poles, a positive HLOSV indicates a westerly wind, and a negative HLOSV indicates an easterly wind; the opposite is true for winds in ~~descending orbit segments. Figure 3 illustrates this zonal wind approximation in the tropics.~~the descending orbit phase. Figure 1 illustrates that in the tropics the HLOSV is approximately equal to the zonal wind in ascending and descending orbit phases. In the left column of Fig. 1, profiles of mean HLOSV for AMVs (solid lines) and Aeolus (long dashed lines) as well as mean AMV wind speed not projected onto the HLOS direction (short dashed lines) are shown. In the center column of Fig. 1, HLOSV MCD (solid lines) and total SDCD (short dashed lines) are plotted as well as the adjusted SDCD with the mean Aeolus L2B uncertainty removed (long dashed lines). Open circles indicate pressure levels at which MCD are statistically significant at the 95% level (p-value < 0.05) using the paired two-sided Student's *t*-test. Corresponding collocation counts are shown in the right column of Fig. 1. The mean AMV and Aeolus HLOSV and their differences exhibit similar magnitudes of opposite sign throughout the vertical between ascending (Fig. ~~3a~~1a-b) and descending (Fig. ~~3d~~1d-e) orbit ~~segments~~phases. This indicates that mean HLOSV differences that include winds from both ascending and descending orbit ~~segments~~phases would be small and would represent differences of larger opposing magnitudes. Moreover, the removal of Aeolus L2B uncertainties ~~(short dashed lines) are~~from the total SDCD results in adjusted SDCD of similar magnitude between

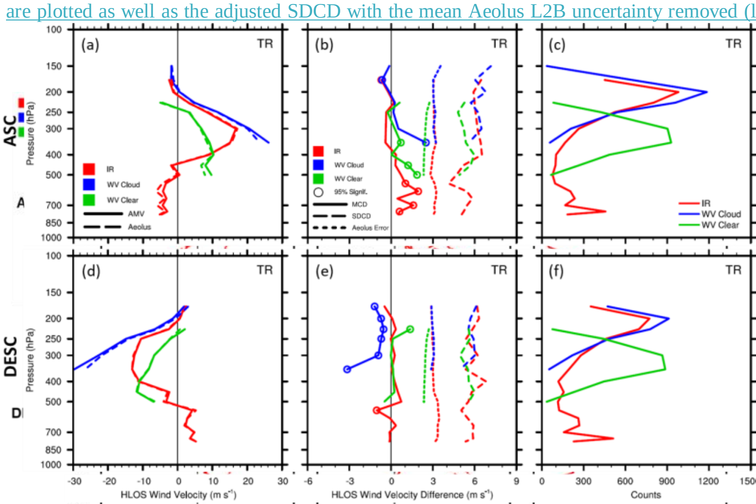

~~**Figure 3: Vertical comparisons of collocated GOES-16 AMVs and RAY winds in the tropics (30° S to 30° N). The top row shows Aeolus ascending orbits, (a) mean AMV (solid lines) and RAY (dashed lines) winds (m s^{-1}), (b) MCD (solid), SDCD (long dashed), and Aeolus L2B uncertainty (short dashed) (m s^{-1}), and (c) collocation counts. (d-f) as in (a-c) but for Aeolus descending orbits. Colors denote AMV channel type: IR (red), WV cloud (blue), and WV clear (green). Colored open circles indicate levels where MCD are statistically significant at the 95% level (p-value < 0.05) using the paired Student's t-test. Vertical zero lines are displayed in the left and center panels in black. Levels with observation counts > 25 are plotted.**~~

MCD are statistically significant at the 95% level (p-value < 0.05) using the paired Student's t-test. Vertical zero lines are displayed in the left and center panels in black. Levels with observation counts > 25 are plotted.

Formatted: Font: Times New Roman
Formatted: Font: Times New Roman
Formatted: Font: Times New Roman
Formatted: Font: Times New Roman
Formatted: Font: Times New Roman
Formatted: Font: Times New Roman
Formatted: Font: Times New Roman
Formatted: Font: Times New Roman
Formatted: Font: Times New Roman
Formatted: Font: Times New Roman
Formatted: Font: Times New Roman

the orbit ~~segments~~phases, implying that the quality of Aeolus winds is not wholly dependent on orbit ~~segment.~~phase during the study period. To simplify the interpretation of the observed HLOS winds, we multiply HLOSV in descending orbit ~~segments~~phases by -1. In doing so, positive HLOSV (away from the poles) now indicates a westerly wind and negative HLOSV an easterly wind, regardless of Aeolus orbit ~~segment~~phase. All statistics in what follows, including Figs. 2, 3, and 5-14, are based on collocation differences that ~~include the combined~~combine ascending and ~~minus~~ -1 times descending orbit phase winds~~. Corresponding statistics are presented in Tables 2-5 and in Fig. 4-9~~.

4 AMV-Aeolus comparison results

In this section we examine in detail the performance of AMVs from the GOES-16 GEO satellite and summarize the AMV performance of all LEO satellites available in the study period. ~~We found~~Here, the reader should keep in mind that performance is relative to Aeolus and for the vector AMV projected onto the Aeolus HLOS. In agreement with previous studies, our results confirm that the level of agreement between AMVs and Aeolus winds varies per combination of conditions including the observing scene type (clear vs. cloudy) coupled with AMV ~~derivation method~~type, geographic region, and height of the observable. Moreover, the findings highlight the value of using Aeolus MIE winds as a comparison standard to characterize AMVs. For context, we begin with summary statistics for samples that include all conditions.

~~Tables~~Figure 2 ~~and 3 summarize~~summarizes the performance of all available GEO AMV HLOS winds ~~from GEO satellites~~ relative to Aeolus RAY (left column) and MIE winds~~, respectively,~~ (right column) in the period of study; likewise, ~~Tables 4 and 5 summarize~~Fig. 3 summarizes LEO AMV performance. The statistics include correlation (*r*), MCD, and SDCD, and ~~root mean squared differences (RMSD) (Wilks, 2011).~~their formulae are listed in Appendix A. The correlation between collocated HLOS winds describes the overall relation of AMVs to Aeolus. The other statistics have their usual meaning (Wilks, 2011) applied to the ~~HLOS wind velocities~~HLOSV. Since the MCD are small compared to the SDCD, the RMSD and SDCD are very similar and in the following we will only discuss the SDCD, but any statement concerning the SDCD also applies to the RMSD. Using the paired two-tailed Student's *t*-test, mean differences significantly different from zero at the 90% (p-value < 0.10) and 95% (p-value < 0.05) confidence levels are indicated ~~by bolded and underlined statistics groupings, respectively. Observation counts are also provided in the tables~~in Figs. 2-3 by striped and solid bars, respectively, and dotted bars indicate the differences are not statistically significant. Observation counts are displayed by grey-blue shading. Direct comparisons between our statistics and those from previous studies are limited because all our statistics are HLOSV, not vector winds. Although we compare mean AMV-Aeolus collocation differences with speed statistics, recall that in general, the HLOS wind generally approximates the zonal component of the horizontal flow rather than the wind speed.

~~Overall, GEO AMVs correspond very well with~~ The main points from the summary collocation statistics of RAY and MIE winds~~, with~~ with AMVs are the following: MIE comparisons exhibit higher correlations and

Formatted: Font: Times New Roman
Formatted: Font: Times New Roman
Formatted: Font: Times New Roman
Formatted: Font: Times New Roman
Formatted: Font: Times New Roman
Formatted: Font: Times New Roman
Formatted: Font: Times New Roman
Formatted: Font: Times New Roman
Commented [KL25]: R2 main point 1
Formatted: Space Before: 12 pt
Formatted: Font: Times New Roman
Formatted: Font: Times New Roman, Font color: Auto
Formatted: Font: Times New Roman, Font color: Auto
Formatted: Font: Times New Roman, Font color: Auto
Formatted: Addition, Font: Times New Roman, 12 pt, Fon color: Auto
Formatted: Font: Times New Roman
Formatted: Font: Times New Roman, Font color: Auto
Formatted: Font: Times New Roman
Formatted: Font: Times New Roman
Formatted: Font: Times New Roman
Formatted: Font: Times New Roman
Formatted: Font: Times New Roman
Commented [KL26]: R2 specific point 14
Formatted: Font: Times New Roman
Formatted: Font: Times New Roman
Formatted: Font: Times New Roman, Italic
Formatted: Font: Times New Roman
Formatted: Font: Times New Roman
Formatted: Font: Times New Roman
Formatted: Font: Times New Roman
Formatted: Font: Times New Roman
Formatted: Font: Times New Roman, Font color: Auto
Formatted: Addition, Font: Times New Roman, Font color Auto
Commented [KL27]: R2 specific point 15

lower SDCD values relative to RAY, reflecting the general higher accuracy of MIE vs. RAY winds. In Fig. 2, GOES and Himawari-8 AMVs having the highest have high correlations with Aeolus (> 0.90). MCD are small and fall within the range of known global GEO wind speed biases (Table 1). The differencesMCD vary depending on the AMV satellite, but are generally smallest in the tropics and largest in the SH extratropics where the SDCD are generally larger by ~1.0 m s^{-1} relative to other regions.larger. For RAY comparisons with GOES and Himawari-8 relative to RAY winds, AMVs, the SDCD range from 5.2827 m s^{-1} in the NH extratropics to 6.5 m s^{-1} in the SH extratropics and fall within the range ofare comparable to wind speed RMSD relative to radiosonderawinsonde winds (see Table 1). Compared to other AMVs, Santek et al., 2019). Of the satellites listed in Fig. 2, Meteosat wind correlations are lowerlowest and corresponding SDCD values are higherhighest by at least 2-3 m s^{-1}.

Performance statistics for LEO AMVs are displayed in Table 4 and Table 5. LEO LEO AMV-Aeolus collocation pairs tend to be found at high latitudes greater than 60° andcollocations in Fig. 3 exhibit statistically significant MCD that fall within range ofare comparable to observed wind speed biases for Aqua and Terra AMVs (see Table 1). Relative to GEO, LEO Key et al., 2016; Le Marshall et al., 2008). AMVs from most LEO satellites exhibit higher SDCD values ofby ~1-2 m s^{-1} for pairs with significant mean differences. Inrelative to GEO, particularly in the Antarctic significant mean HLOSV differences have highwhere SDCD values are on the order of 7.5-8.5 m s^{-1} for RAY and 65.9-7.5 m s^{-1} for MIE. MIE comparisons in all regions exhibit higher correlations and lower SDCD values relative to RAY comparisons, reflecting the general higher accuracy of MIE vs. RAY winds. Another possible reason is that MIE comparisons might generally have smaller collocation errors.

Formatted: Font: Times New Roman
Formatted: Font: Times New Roman
Formatted: Font: Times New Roman
Formatted: Font: Times New Roman
Formatted: Font: Times New Roman
Formatted: Font: Times New Roman
Formatted: Font: Times New Roman
Formatted: Font: Times New Roman
Formatted: Font: Times New Roman
Formatted: Font: Times New Roman
Formatted: Font: Times New Roman
Formatted: Font: Times New Roman
Formatted: Font: Times New Roman
Formatted: Font: Times New Roman
Formatted: Font: Times New Roman
Formatted: Font: Times New Roman
Formatted: Font: Times New Roman
Formatted: Font: Times New Roman
Formatted: Font: Times New Roman
Formatted: Font: Times New Roman
Formatted: Font: Times New Roman
Formatted: Font: Times New Roman
Formatted: Font: Times New Roman

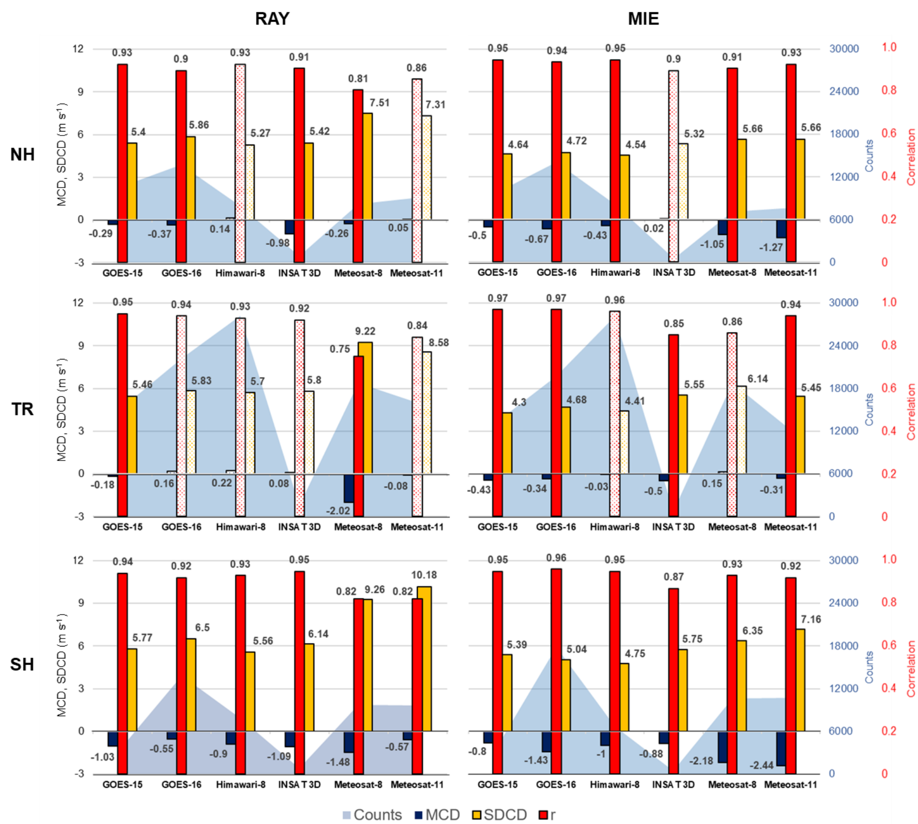

Figure 2: AMV-Aeolus MIE winds represent cloudy scenes, and IR window and WVcloud AMVs require clouds to track motions. As Aeolus RAY winds represent clear-sky and must be cloud-free, the global mean great circle collocation distances tend to be slightly larger for RAY than MIE (59.5 km and 51.2 km, respectively).

Formatted: TBD, Font: Times New Roman, Font color: Te 1

Formatted: TBD, Font: Times New Roman, Font color: Te 1

Table 2: Summary of performance characteristics of all collocations of quality-controlled GEO AMVs and quality-controlled Aeolus Rayleigh-clear (RAY) winds during the study period (2 August 2019 to 16 September 2019). Statistics statistics in the (top row) NH, (middle row) tropics (TR), and (bottom row) SH for GEO satellites that include correlation (r),) in red, mean collocation differencesdifference (MCD) between the HLOS winds (AMV-Aeolus) in m s^{-1}navy blue, standard deviation of the collocation differences (SDCD) in m s^{-1}, root mean squared difference (RMSDSDCD) in m s^{-1}, and collocation count. Statistics are based on AMV minus Aeolus differences for all available AMV channel types for each Aeolus mode and at all vertical levels, and are stratified by GEO satellite and by geographic region (defined by boundaries at 30° S and 30° N), with NH indicating the Northern Hemisphere extratropics, TR the tropics, and SH the Southern Hemisphere extratropics. Bolded and bolded/underlined statistics yellow, and collocation counts as light blue shaded areas. Solid colors denote collocation groupings with statistically significant mean HLOSV differences at the 90% level (p-value < 0.10) and the 95% level (p-value < 0.05), respectively. A two-sided single-variance Student's t-test is used to ascertain statistical significance based on the null hypothesis that the two sample populations have the same mean, stripes denote 90% statistical significance, and dots indicate the differences are not statistically significant.

Geographic Region	GEO Satellite	r	MCD (m s^{-1})	SDCD (m s^{-1})	RMSD (m s^{-1})	Count
NH	GOES-15	0.93	-0.29	5.40	5.40	10823
NH	GOES-16	0.90	-0.35	5.86	5.87	13912
NH	Himawari-8	0.93	0.13	5.28	5.28	8048
NH	INSAT-3D	0.91	-0.98	5.41	5.50	934
NH	Meteosat-8	0.81	-0.26	7.52	7.53	8302
NH	Meteosat-11	0.86	0.04	7.31	7.31	9234
TR	GOES-15	0.95	-0.17	5.46	5.46	15577
TR	GOES-16	0.94	0.17	5.82	5.83	22478
TR	Himawari-8	0.93	0.22	5.70	5.71	28494
TR	INSAT-3D	0.92	0.07	5.80	5.80	1588
TR	Meteosat-8	0.75	-2.03	9.22	9.44	18934
TR	Meteosat-11	0.84	-0.07	8.58	8.58	16198
SH	GOES-15	0.94	-1.04	5.76	5.85	3949
SH	GOES-16	0.92	-0.55	6.51	6.54	14072

Formatted: Don't keep with next
Formatted: TBD, Font color: Text 1
Formatted: TBD, Font color: Text 1
Formatted: TBD, Font color: Text 1
Formatted: TBD, Font color: Text 1
Formatted: TBD, Font color: Text 1
Formatted: TBD, Font color: Text 1
Formatted: TBD, Font color: Text 1
Formatted: TBD, Font color: Text 1
Formatted: TBD, Font color: Text 1
Formatted: TBD, Font color: Text 1
Formatted: TBD, Font color: Text 1
Formatted: TBD, Font color: Text 1
Formatted: Font color: Text 1

SH	Himawari-8	0.92	-0.92	5.56	5.63	7906
SH	INSAT-3D	0.95	-1.10	6.13	6.22	784
SH	Meteosat-8	0.82	-1.48	9.26	9.38	9817
SH	Meteosat-11	0.82	-0.57	10.18	10.20	9705

Table 3: As in Table 2, but for Aeolus Mie-cloudy (MIE) winds.

Geographic Region	*GEO Satellite*	*r*	*MCD ($m\ s^{-1}$)*	*SDCD ($m\ s^{-1}$)*	*RMSD ($m\ s^{-1}$)*	*Count*
NH	GOES-15	0.95	-0.49	4.63	4.66	10032
NH	GOES-16	0.94	-0.67	4.72	4.77	14301
NH	Himawari-8	0.95	-0.42	4.54	4.56	8237
NH	INSAT-3D	0.90	-0.01	5.32	5.32	476
NH	Meteosat-8	0.91	-1.05	5.66	5.76	7143
NH	Meteosat-11	0.93	-1.27	5.66	5.80	7719
TR	GOES-15	0.97	-0.43	4.29	4.31	13575
TR	GOES-16	0.97	-0.32	4.68	4.69	19945
TR	Himawari-8	0.96	-0.04	4.41	4.41	28511
TR	INSAT-3D	0.86	-0.52	5.53	5.55	796
TR	Meteosat-8	0.86	0.14	6.14	6.14	18976
TR	Meteosat-11	0.94	-0.31	5.45	5.46	12262
SH	GOES-15	0.95	-0.79	5.38	5.44	4097

SH	GOES-16	0.96	-1.42	5.05	5.25	18157
SH	Himawari-8	0.95	-1.03	4.79	4.90	6798
SH	INSAT-3D	0.87	-0.88	5.73	5.79	438
SH	Meteosat-8	0.93	-2.19	6.34	6.71	10699
SH	Meteosat-11	0.92	-2.45	7.15	7.56	10804

Table 4: As in Table 2 but for differences between LEO IR-window AMVs and Aeolus Rayleigh-clear (RAY) winds in the Arctic (north of 60° N) and Antarctic (south of 60° S) polar regions.

Geographic Region	*LEO Satellite*	*r*	*MCD* ($m\ s^{-1}$)	*SDCD* ($m\ s^{-1}$)	*RMSD* ($m\ s^{-1}$)	*Count*
Arctic	Aqua	**0.89**	**-0.90**	**6.54**	**6.60**	**546**
Arctic	MetOp-A	0.87	-0.07	6.58	6.58	1530
Arctic	MetOp-B	0.87	-0.11	6.61	6.60	1647
Arctic	NOAA-15	0.88	-0.12	6.78	6.77	249
Arctic	NOAA-18	0.88	-0.09	6.39	6.37	190
Arctic	NOAA-19	**0.84**	**-0.68**	**6.40**	**6.42**	**249**
Arctic	NOAA-20	**0.91**	**-0.29**	**6.46**	**6.46**	**2642**
Arctic	S-NPP	**0.91**	**-0.32**	**6.49**	**6.49**	**1894**
Arctic	Terra	**0.88**	**-0.37**	**6.45**	**6.46**	**988**
Antarctic	Aqua	0.92	0.28	8.22	8.22	1201
Antarctic	MetOp-A	**0.88**	**-0.46**	**8.51**	**8.52**	**1471**
Antarctic	MetOp-B	**0.88**	**-0.59**	**8.36**	**8.37**	**1788**
Antarctic	NOAA-15	0.88	-0.77	9.79	9.80	249
Antarctic	NOAA-18	0.87	-0.66	10.57	10.56	172
Antarctic	NOAA-19	0.82	-0.35	11.16	11.16	836
Antarctic	NOAA-20	**0.94**	**-0.73**	**8.17**	**8.20**	**2667**
Antarctic	S-NPP	**0.95**	**-0.76**	**7.49**	**7.53**	**2384**
Antarctic	Terra	0.88	-0.10	9.32	9.31	996

430

Table 5: As in Table 4 but for Aeolus Mie-cloudy (MIE) winds.

Geographic Region	*LEO Satellite*	*r*	*MCD ($m\ s^{-1}$)*	*SDCD ($m\ s^{-1}$)*	*RMSD ($m\ s^{-1}$)*	*Count*
Arctic	Aqua	0.94	-0.54	5.24	5.26	848
Arctic	MetOp-A	0.92	-0.54	5.61	5.63	3311
Arctic	MetOp-B	0.93	-0.56	5.09	5.12	3650
Arctic	NOAA-15	0.93	-0.30	4.92	4.92	375
Arctic	NOAA-18	0.93	-0.72	5.08	5.13	336
Arctic	NOAA-19	0.90	-0.12	5.15	5.15	395
Arctic	NOAA-20	0.94	0.03	5.17	5.17	5225
Arctic	S-NPP	0.94	0.09	5.30	5.30	4006
Arctic	Terra	0.94	-0.57	4.76	4.79	1689
Antarctic	Aqua	0.94	0.21	6.89	6.89	1065
Antarctic	MetOp-A	0.93	-0.44	7.51	7.52	1761
Antarctic	MetOp-B	0.93	-0.67	6.74	6.77	2142
Antarctic	NOAA-15	0.95	-0.83	5.95	6.00	291
Antarctic	NOAA-18	0.95	-0.14	6.37	6.36	231
Antarctic	NOAA-19	0.92	-0.13	7.88	7.88	930
Antarctic	NOAA-20	0.97	-0.72	6.31	6.35	4537
Antarctic	S-NPP	0.97	-0.73	6.40	6.44	4356
Antarctic	Terra	0.92	-0.08	7.13	7.13	958

Differences in the SH extratropics and Antarctic pole exhibit higher SDCD values compared with the rest of the globe. This is likely due to several factors. During the study period, the SH region of GEO fields-of-view covers a portion of the winter storm tracks that propagate eastward all the way around the Southern Ocean. The SH storm tracks exist year-round, and in winter (June-July-August) the upper-tropospheric subtropical jet is stronger and acts as a waveguide for eastward propagating baroclinic waves over a broader latitude range (Trenberth, 1991; Nakamura and Shimpo, 2004; Hoskins and Hodges, 2005), thus ~~enhancing~~amplifying wind shear and storm track intensity. This is one factor that explains the higher SDCD values observed in GEO differences in the SH extratropics, as AMV uncertainties tend to increase with increasing wind speed (Posselt et al., 2019) and high wind shear (Bormann et al., 2002; Cordoba et al., 2017). In the Antarctic polar region, the general strengthening of the polar vortex aloft in late winter/early spring (i.e., during the study period) is related to a stronger equator-pole temperature gradient brought about by gradually increasing subtropical lower stratospheric temperatures from March to September (Zuev and Savelieva, 2019). A stronger Antarctic polar vortex is associated with stronger zonal winds aloft (and ~~thus~~ stronger ~~wind~~ shear) which ~~would limit accurate AMV and Aeolus wind retrievals, thereby increasing~~could increase the corresponding SDCD values ~~on both accounts~~for AMVs due to the wind-shear height assignment error effect. Surface effects may also play a role, as very cold brightness temperatures at or near the polar surface may be misinterpreted as ~~very high~~ cloud tops due to the low temperature contrast between clouds and the surface snow or ice (Key et al., 2016).

Formatted: Font: Times New Roman

Formatted: Font: Times New Roman

Formatted: Font: Times New Roman

Formatted: Font: Times New Roman

Formatted: Font: Times New Roman

Formatted: Font: Times New Roman

Formatted: Font: Times New Roman

~~Section 4.1 compares GOES-16 AMVs with Aeolus HLOS winds. We chose to examine GOES-16 AMVs~~

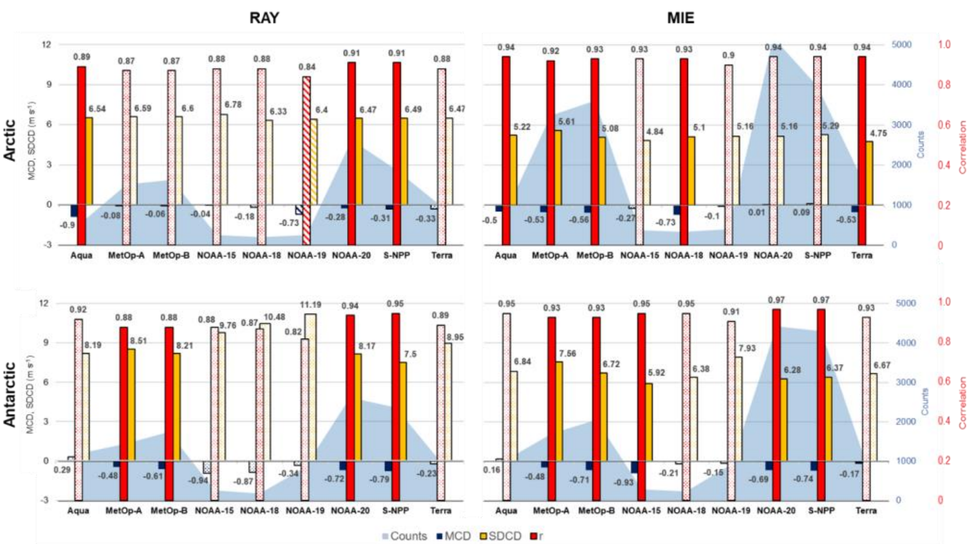

Figure 3: As in Fig. 2 but for LEO satellites.

As a case study, we examine in greater detail the performance of AMVs from GOES-16, a GEO satellite (Section 4.1). This is done because compared with other GEO satellites, GOES-16 exhibits high correlations with Aeolus RAY (> 0.90) and MIE winds (> 0.94), relatively small SDCD (5.~~82~~8-6.~~51~~5 m s^{-1} for RAY, 4.~~72~~7-5~~.05~~ m s^{-1} for MIE), and have the largest extratropical sample size from which to compute robust statistics (see ~~Table~~Fig. 2~~ and Table 3~~). The other GEO satellites are not further examined as they exhibit larger RAY SDCD (Meteosat-8 and -11), have a much smaller extratropical sample size (Himawari-8, ~~INSAT 3D,~~ Meteosat-8 and -11), or ~~have transitioned out of main~~are not actively used in NCEP operations (GOES-15~~). Section 4.2 discusses~~ and INSAT 3D). GOES-16 AMVs are derived from full disk images centered at 75.2° W longitude from the ~~comparison~~onboard Advanced Baseline Imager (ABI). GOES-16 cloud-top AMVs are generally of good quality and when validated against rawinsonde winds exhibit a relatively small mean difference in wind speed ranging from -1.0 m s^{-1} to +0.5 m s^{-1} and mean vector differences of ~~all available LEO AMVs~~ 3-6 m s^{-1} that tend to increase with height (Daniels et al., 2018). Figure 4 presents the GOES-16/Aeolus collocation number densities (i.e., the total number of collocated observation pairs within each grid cell on a 1.25° (~140 km) resolution map) covering the period of study. QC'd GOES-16 AMVs collocated with QC'd RAY and MIE winds are shown in Fig. 4a and Fig. 4b, respectively. MIE collocations exhibit three bands of high-density winds along the intertropical convergence zone (ITCZ) and extratropical storm tracks, with few

Formatted: Normal, Left, Line spacing: single
Formatted: Font: Times New Roman
Formatted: Font: Times New Roman
Formatted: Font: Times New Roman
Formatted: Font: Times New Roman
Formatted: Font: Times New Roman
Formatted: Font: Times New Roman
Formatted: Font: Times New Roman
Formatted: Font: Times New Roman
Formatted: Font: Times New Roman
Formatted: Font: Times New Roman
Formatted: Font: Times New Roman
Formatted: Font: Times New Roman
Formatted: Font: Times New Roman
Formatted: Font: Times New Roman
Formatted: Font: Times New Roman
Formatted: Font: Times New Roman
Formatted: Font: Times New Roman
Formatted: Font: Times New Roman

winds found between 0-30° S. A similar but smoother version of the MIE distributions is shown for collocated RAY winds. The MIE collocation number density is greater than that for RAY, as AMV observation density tends to be higher in very cloudy or very moist scenes (Velden et al., 1997).

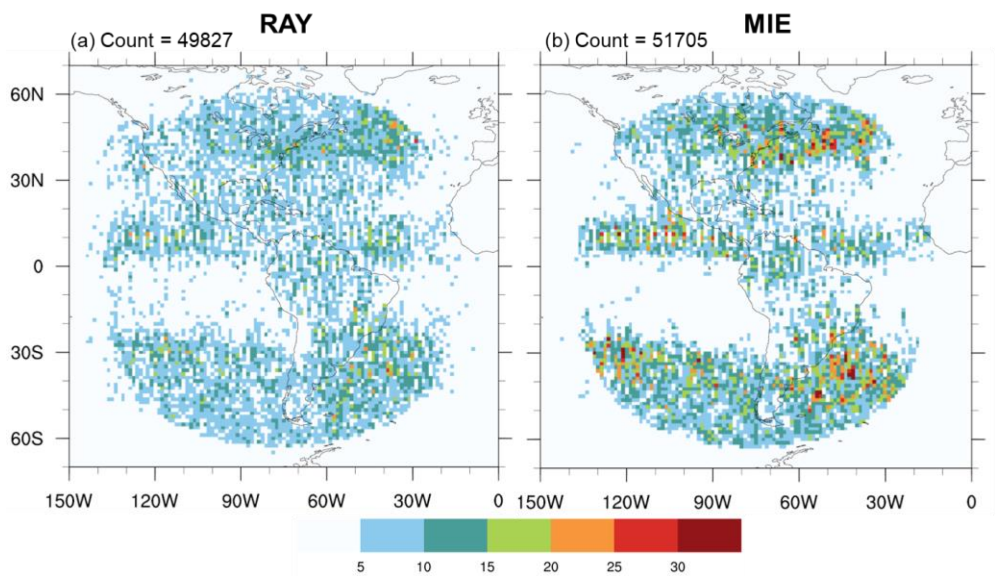

Figure 4: Number densities of quality-controlled GOES-16 AMV observations collocated with quality-controlled Aeolus (a) Rayleigh-clear (RAY), and (b) Mie-cloudy (MIE) HLOS winds. Colors indicate total number of collocated observation pairs within a grid cell at 1.25° (140 km) horizontal resolution. Total observation count per panel is displayed at the top left corner. This and all subsequent plots are for all collocations with quality controlled AMV and Aeolus winds during the study period (2 August 2019 to 16 September 2019).

Formatted: Font: Times New Roman

Formatted: Font: Times New Roman

For the LEO perspective, we choose to examine the performance of all LEO IR AMVs rather than from a single satellite (Section 4.2). This is done because compared to GEO, LEO AMVs from each satellite comprise a relatively small sample of collocated winds, and this would render any associated performance metrics unreliable. Further, unlike the suite of available GEO satellites where each observe a different region of the globe (except for small areas where the footprints of neighboring satellites overlap), each LEO satellite observes AMVs in the same polar regions and thus samples the same atmospheric motions. Figure 5 depicts observation number densities of QC'd LEO AMVs collocated with QC'd RAY and MIE winds in the Arctic and Antarctic polar regions bounded by 60° latitude: Arctic RAY (Fig. 5a), Arctic MIE (Fig. 5b), Antarctic RAY (Fig. 5c), and Antarctic MIE (Fig. 5d). In general, more LEO/MIE collocation pairs pass QC and are retained in the analysis than for RAY winds. Collocations in the Arctic are found across the high latitudes with MIE comparisons exhibiting higher concentrations poleward of Eurasia and North America. Antarctic collocations are primarily found over the western half of the continent. In this region, water vapor features are more suitable for tracking and deriving AMVs as they exist downstream of intense upper-level storm tracks (Hoskins and Hodges, 2005) in an area of higher annual precipitation (Grieger et al., ~~detects the same atmospheric motions.~~ 2016).

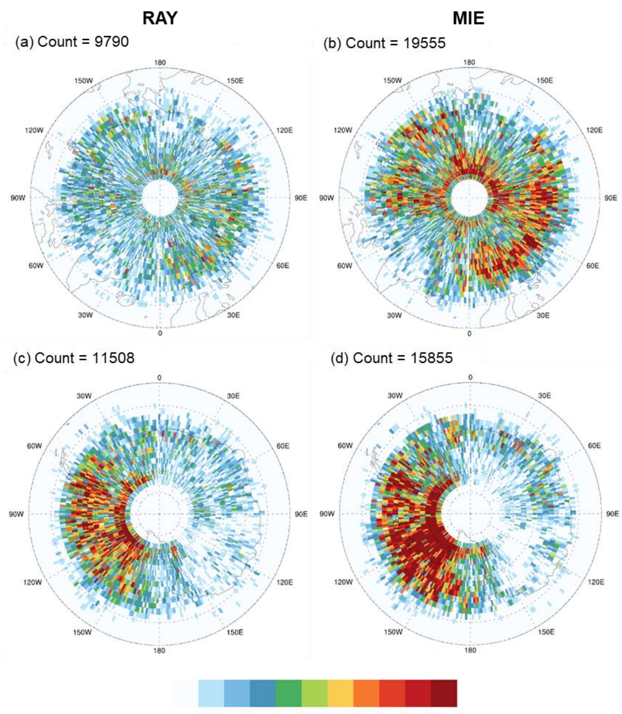

Figure 5: Number densities of IR-derived AMVs from all available LEO satellites collocated with Aeolus RAY (left, a, c) and MIE (right, b, d) winds in the (a, b) Arctic (north of 60° N), and (c, d) Antarctic (south of 60° S). Colors indicate total number of collocated observation pairs within a grid cell at 1.25° (approximately 140 km in the N-S direction) horizontal resolution. Dashed latitude lines are spaced every 5 degrees. Total observation count per panel is displayed at the top left corner.

Formatted: Font: Times New Roman

Formatted: Font: Times New Roman

4.1 GOES-16 AMVs vs. Aeolus

To increase the size of our collocation data set, we compared all types of GOES-16 AMVs to both Rayleigh-clear and Mie-cloudy winds. In addition, we do not show results from WVclear AMV collocations with Mie-cloudy winds as correlations for this category of collocations are poor and the sample size is very small (see Table 1), and this result may be unreliable. With a larger data set it might be possible to compare Rayleigh-clear and Mie-cloudy winds to clear and cloudy AMVs only, respectively. Additionally, winds retrieved from tracking clear-sky and cloud motions represent different dynamical features and tend to behave differently. For example, the recommended time interval for tracking cloud motions is 10-15 minutes to capture short cloud lifetimes and rapid intensification/deformation, while the recommended time interval for clear-air motions of 30 minutes is suitable to capture variations in jet streams and other clear-air features (Schmetz et al., 2000).

4.1.1 Rayleigh-clear (RAY) comparisons

Figure ~~4 presents~~6 depicts density scatterplots that summarize the relationship of GOES-16 AMVs to RAY winds ~~stratified by geographic region and AMV method~~ to highlight the regional differences in IR (Fig. ~~4a, 4d, 4g~~6a, 6d, 6g), WVcloud (Fig. ~~4b, 4e, 4h~~6b, 6e, 6h), and WVclear AMVs (Fig. ~~4c, 4f, 4i~~6c, 6f, 6i). Sample statistics are based on Aeolus as the reference dataset and are displayed in the lower right of each panel. AMVs are highly correlated with RAY winds (0.88-0.91 in the extratropics and 0.93-0.95 in the tropics), with most collocations for each AMV type falling close to the one-to-one line that indicates a perfect match. Note that in the NH and SH extratropics, most collocations are found in the upper-right quadrant~~.~~ where HLOS winds ~~in this quadrant~~ are of positive sign~~, indicating~~ and indicate the dominant westerly flow ~~which is the dominant direction~~ of ~~motion in the general circulation in~~ the extratropics. In the tropics, ~~maximum densities~~many collocations are ~~found~~grouped in the lower-left quadrant ~~(small negative HLOS) as well as the~~ that indicates the easterly flow of the tropical trade winds at lower levels, and the rest are found in the upper-right quadrant~~. The negative HLOS winds in the lower-left quadrant indicate easterly flow~~ that represents ~~the tropical trade winds at lower levels, while the positive HLOS winds in the upper-right quadrant represent more~~ westerly tropical flow at upper levels. Of ~~(e.g., see Fig. 5d).~~

~~AMVs correspond well with RAY winds with correlations of 0.88-0.9 in the extratropics and 0.94 in~~ the ~~tropics. Note that most of~~three AMV types, the ~~collocations for each AMV channel type fall close to the one-to-one line that indicates a perfect match. The~~ best match is for WVclear AMVs ~~and RAY winds.~~, with the comparisons exhibiting the smallest SDCD values in each geographic region, that in turn are comparable to known wind speed SD and RMS of all GEO AMVs relative to rawinsonde winds (Santek et al., 2019). This is expected~~, as it is a comparison of winds obtained by tracking upper-tropospheric features in clear air with~~ since WVclear AMVs and Aeolus RAY winds ~~retrieved in nearby~~are most probably sampling similar clear-sky scenes, and clear scenes are more homogeneous over time and space scales, which in turn implies smaller collocation differences. ~~WVclear AMVs exhibit the smallest SDCD values in each geographic region, and these fall within the range of known speed SD and RMS of all GEO AMVs relative to radiosonde winds (see Table 1). The smallest WVclear SDCD are found in the tropics where mean HLOSV is smallest around 7 m s^{-1}.~~ Ideally, one would expect samples large enough to provide

Formatted: Space Before: 6 pt

Commented [KL28]: R1 point 7, R2 specific point 18

Formatted: Space Before: 6 pt

Formatted: TBD, Font color: Auto

statistically significant collocation differences between RAY winds and WVclear AMVs only; as it turns out, collocation differences are also statistically significant for IR and WVcloud comparisons show similar relationships with larger MCD and SDCD estimates. The largest SDCD in WVclear AMVs are found in the SH extratropics where mean HLOSV is fastest around 20 m s^{-1}. Higher wind speeds (and most probably stronger wind shear) observed in the SH extratropics for all AMV channels can reduce the accuracy of both AMV derivations and Aeolus wind retrievals. The results suggest that the relationship of AMVs to RAY profiles characterizes known AMV uncertainty in clear scenes in the tropics and NH extratropics similar to high quality sources of wind profile observations. The certainty of such a statement for motions in the SH extratropics is more difficult to verify, as there are much fewer radiosonde observations available in the Southern Hemisphere for comparison (e.g., Durre et al., 2006, their Fig. 1). Further, it can be inferred that QC'd WVclear AMVs represent well the dynamical flow in clear scenes in the tropics, particularly in summer where there is high moisture content available for tracking upper-level clear-sky water vapor features (Velden et al., 1997).AMVs (see Fig. 7). In these cases cloudy AMVs are collocated with Aeolus RAY winds that represent clear scenes, and since they do not observe the same type of scene, Aeolus and/or AMV representativeness errors are most probably larger (hereafter we refer to this as the cloudy/clear sampling effect).

We next examine theFigure 7 presents mean vertical variationprofiles of AMV minusGOES-16 AMVs and Aeolus RAY winds (, and corresponding MCD and SDCD distributions, similar to what is shown in Fig. 5).1. This perspective has the potential to can provide additional insight into how well each AMV channel represents the the accuracy of AMVs in representing the mean horizontal flow at various vertical levels.throughout the atmospheric column. Mean vertical profiles of QC'd GOES-16 AMV and RAY HLOSV and their mean differences and SDCD are plotted per AMV channel type in the NH extratropics (Fig. 5a7a-c), tropics (Fig. 5d7d-f), and SH extratropics (Fig. 5g7g-i). In Fig. 5a, 5dFigs. 7a, 7d, and 5g, profiles of mean7g, AMV HLOSV for AMVs (solid lines) and Aeolus (HLOSV (long dashed lines) generally show good agreement. In Fig. 5b, 5e at all latitudes, and 5h, mean differences in large gradients of HLOSV (solid lines) and standard deviationscorrespond to layers of strong vertical wind shear inferred by the differences (long dashed lines) are shown as well as higher rate of change of AMV wind speed in the mean Aeolus L2B uncertainty vertical (short dashed lines), with open circles indicating pressure levels at which HLOSV differences). Corresponding MCD are statistically significant at the 95% level (p-value < 0.05) using the paired two-sided Student's *t*-test. Corresponding most levels at all latitudes (Figs. 7b, 7e, and 7h) and seem to depict known AMV biases relative to high-quality sources of wind profile observations, particularly outside of the SH. For example, in the NH extratropics, MCD range from -0.5 to -1.0 m s^{-1} at levels where collocation counts are shown in Fig. 5c, 5f, and 5i.

Formatted: TBD, Font: 12 pt, Font color: Auto

Commented [KL29]: R2 specific point 17

Formatted: TBD, Font: 12 pt, Bold, Font color: Auto, Engl (United Kingdom)

Formatted: TBD, Font color: Auto

Formatted: TBD, Font color: Auto

Formatted: TBD, Font color: Auto

Formatted: TBD, Font color: Auto

Formatted: TBD, Font color: Auto

Formatted: TBD, Font color: Auto

Formatted: TBD, Font color: Auto

Formatted: TBD, Font color: Auto

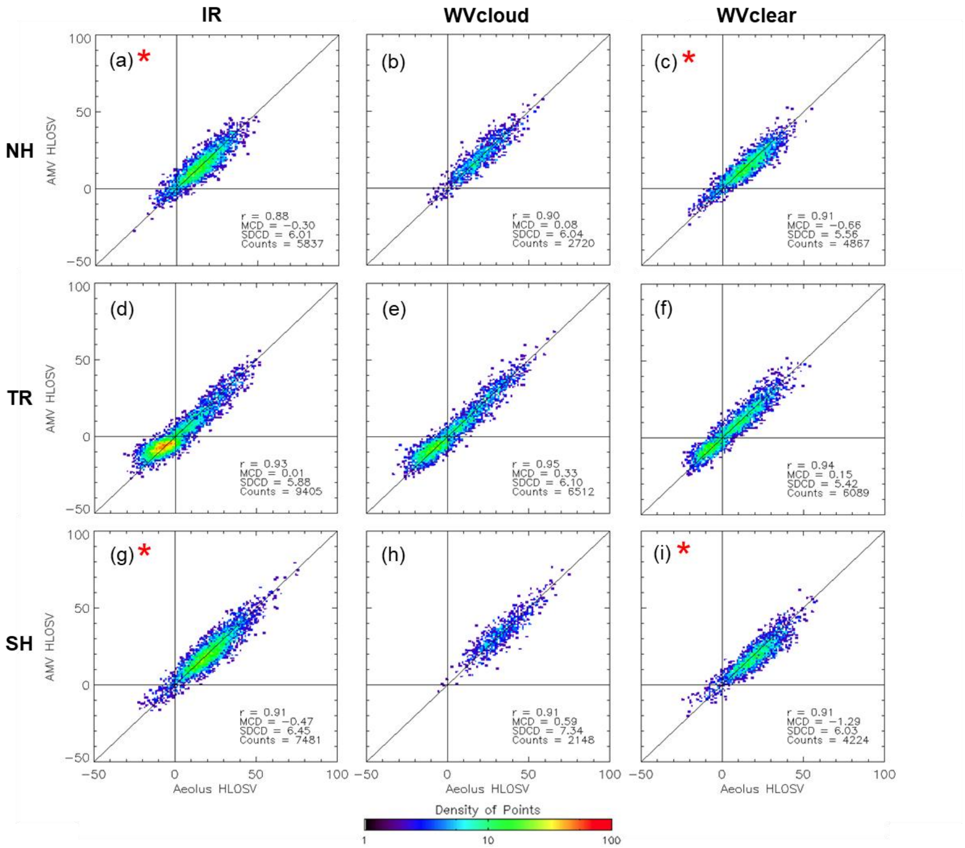

Figure 6: Density scatterplot of collocated GOES-16 AMVs and RAY winds. Rows are for the (top, a-c) NH extratropics (30-60° N), (middle, d-f) tropics (TR) (30° S to 30° N), and (bottom, g-i) SH extratropics (30-60° S). Columns are for different AMV channel types: (left, a, d, g) IR, (center, b, e, h) WVcloud, and (right, c, f, i) WVclear. Colors indicate total number of collocated observation pairs within the cells plotted, which are 1 ms^{-1} on a side. Sample statistics are displayed in the bottom right corner of each panel. Horizontal and vertical zero lines are plotted in black, as is the diagonal one-to-one line. Red star denotes statistical significance at 95% using the paired two-tailed Student's t-test. HLOSV units are m s^{-1}.

Vertical profiles of AMV peak and could represent a small slow AMV bias as previously noted by Bormann et al. (2002). RAY HLOSV closely match in each geographic region. HLOSV increases with height, with NH speeds peaking at 20 m s^{-1} near In the jet stream level (~250 hPa) and decreasing aloft, and with SH speeds continuously increasing with height to more than 30tropics, AMVs exhibit an apparent small fast bias, that is the positive MCD of 0.5 to 1.0 m s^{-1} at the highest levels. Large HLOSV in the extratropics at upper levels correspond to a deep layer of enhanced vertical wind shear , that could be associated with the corresponding jets and storm tracks captured in the northern and southern regions as viewed by GOES-16; the larger HLOSV in the SH indicate faster motions and strongerlarger AMV errors (and larger Aeolus errors) in layers of high winds and strong vertical wind shear in the winter hemisphere.(Cotton et al., 2020).

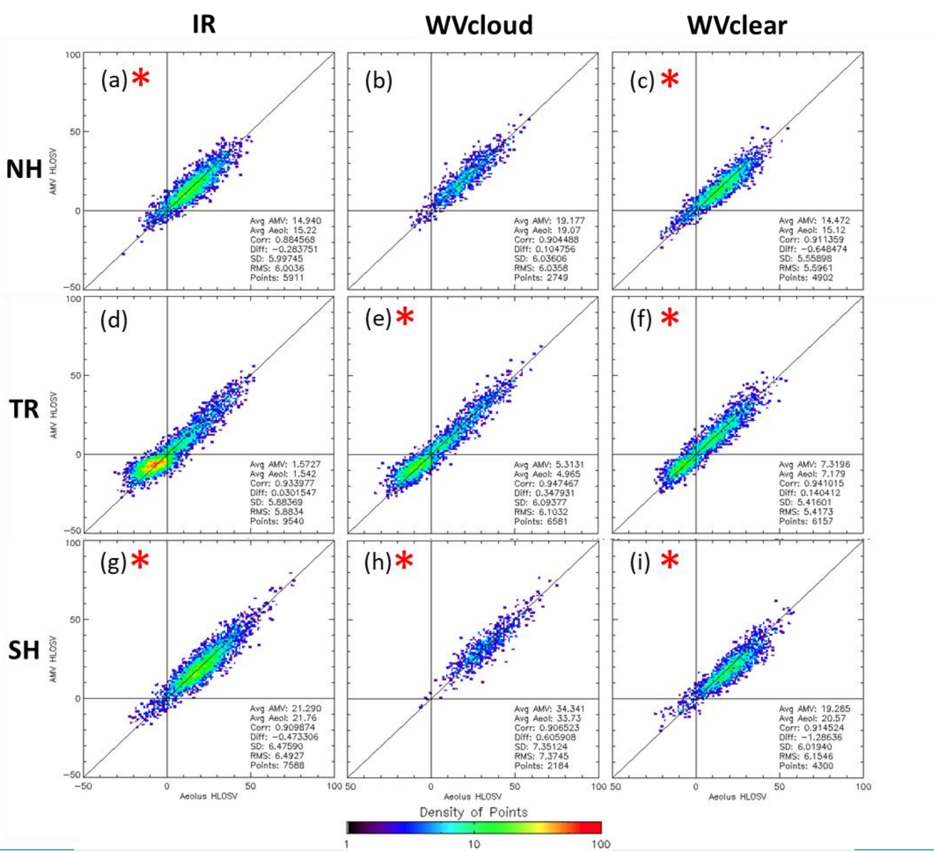
IR
WVcloud
WVclear
NH
TR
SH
(a) *
(b)
(c) *
(d)
(e) *
(f) *
(g) *
(h) *
(i) *
AMV HLOSV
Aeolus HLOSV
Avg AMV: 14.940
Avg Aeol: 15.22
Corr: 0.884568
Diff: −0.283751
SD: 5.99745
RMS: 6.0036
Points: 5911
Avg AMV: 19.177
Avg Aeol: 19.07
Corr: 0.904488
Diff: 0.104756
SD: 6.03606
RMS: 6.0358
Points: 2749
Avg AMV: 14.472
Avg Aeol: 15.12
Corr: 0.911359
Diff: −0.648474
SD: 5.55898
RMS: 5.5961
Points: 4902
Avg AMV: 1.5727
Avg Aeol: 1.542
Corr: 0.933977
Diff: 0.0301547
SD: 5.88369
RMS: 5.8834
Points: 9540
Avg AMV: 5.3131
Avg Aeol: 4.965
Corr: 0.947467
Diff: 0.347931
SD: 6.09377
RMS: 6.1032
Points: 6581
Avg AMV: 7.3196
Avg Aeol: 7.179
Corr: 0.941015
Diff: 0.140412
SD: 5.41601
RMS: 5.4173
Points: 6157
Avg AMV: 21.290
Avg Aeol: 21.76
Corr: 0.909874
Diff: −0.473306
SD: 6.47590
RMS: 6.4927
Points: 7588
Avg AMV: 34.341
Avg Aeol: 33.73
Corr: 0.906523
Diff: 0.605908
SD: 7.35124
RMS: 7.3745
Points: 2184
Avg AMV: 19.285
Avg Aeol: 20.57
Corr: 0.914524
Diff: −1.28636
SD: 6.01940
RMS: 6.1546
Points: 4300
Density of Points
1
10
100

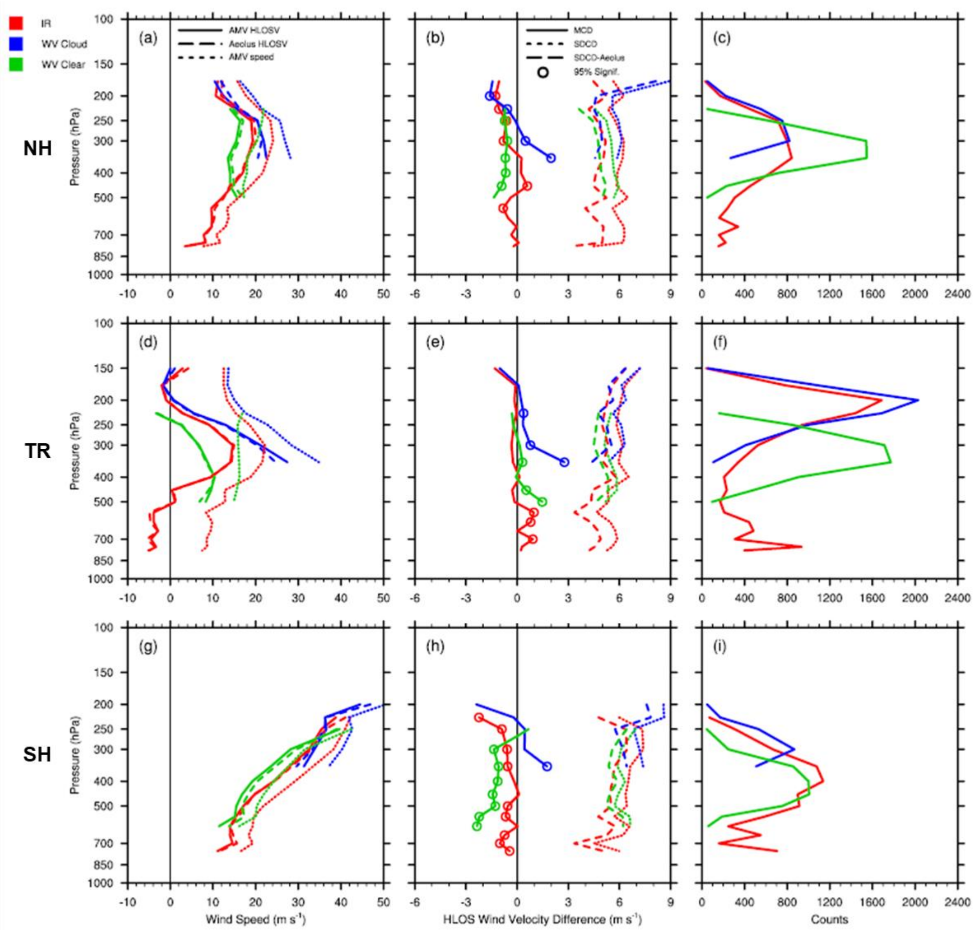

Figure 7: Density scatterplot of collocated GOES-16 AMVs and RAY winds. Rows are for the (a-c) NH extratropics (30-60° N), (d-f) tropics (TR) (30° S to 30° N), and (g-i) SH extratropics (30-60° S). Columns are for different AMV channel types: (left) IR, (center) WVcloud, and (right) WVclear. Colors indicate total number of collocated observation pairs within the cells plotted, which are 1 ms^{-1} on a side. Sample statistics are displayed in the bottom right corner of each panel. Horizontal and vertical zero lines are plotted in black, as is the diagonal one-to-one line. Red star denotes statistical significance at 95% using the paired two-tailed Student's t-test. HLOSV units are m s^{-1}.

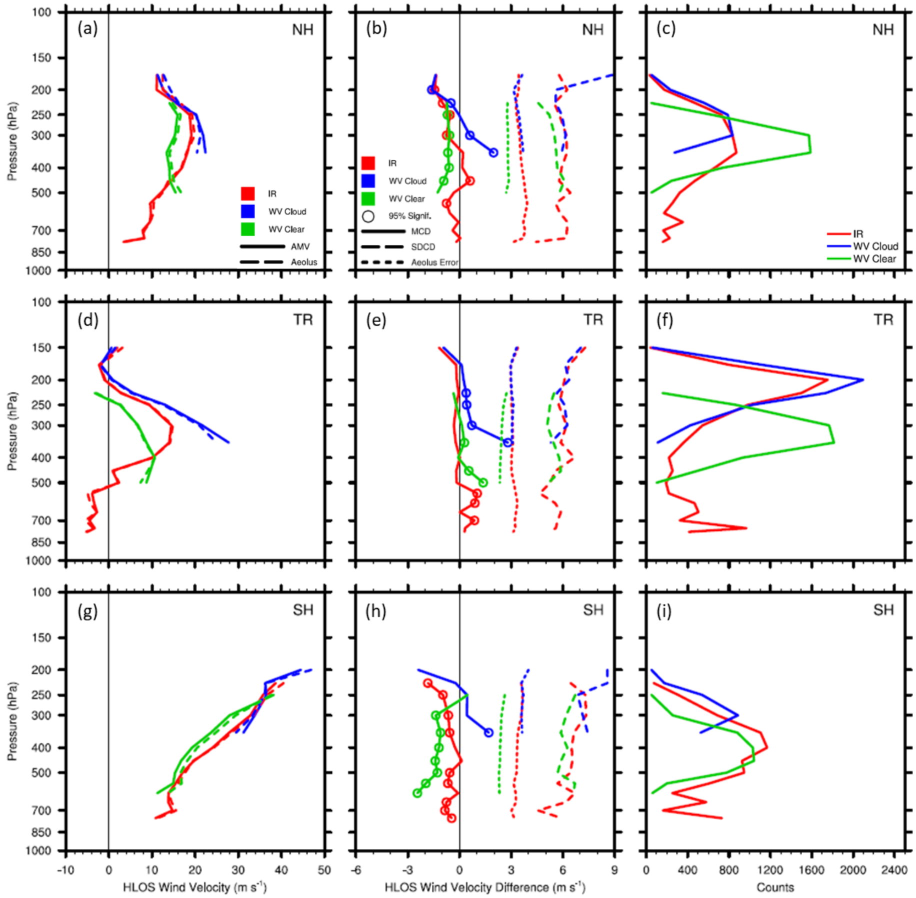

~~Figure 5: Vertical comparisons~~: Vertical profiles of collocated GOES-16 AMVs and RAY winds. The top row shows the NH extratropics (30-60° N), (a) mean AMV HLOSV (solid lines~~) and~~), RAY (HLOSV (long dashed lines~~) winds~~), and mean AMV wind speed (short dashed lines) (m s^{-1}~~),~~); (b) MCD (solid), SDCD (~~long~~short dashed), and AMV HLOSV error as represented by SDCD-Aeolus L2B uncertainty (~~short~~long dashed) (m s^{-1}~~),~~); and (c) collocation counts. (d-f) as in (a-c) but for the tropics (30° S to 30° N), and (g-i) as in (a-c) but for the SH extratropics (30-60° S). Colors denote AMV ~~channel~~ type: IR (red), WV cloud (blue), and WV clear (green). Colored open circles indicate levels where MCD are statistically significant at the 95% level (p-value < 0.05) using the paired Student's *t*-test. Vertical zero lines are displayed in the left and center panels in black. Levels with observation counts > 25 are plotted.

Formatted: Font: Italic

Formatted: TBD, Font: 10 pt

HLOSV differences are statistically significant throughout the vertical in all geographic regions and exhibit similar vertical behavior in both extratropical regions and opposing behavior in the tropics. In the NH and SH extratropics at levels where collocation counts peak, mean HLOSV collocation differences are small (-1.0 m s^{-1} to -2.0 m s^{-1}) yet statistically significant and could represent a small slow AMV bias which has been previously noted by Bormann et al. Profiles of the total RAY SDCD (short dashed lines in Figs. 7b, 7e, and 7h) that include AMV errors, Aeolus errors, and collocation/representativeness errors exhibit rather large values (> 6 m s^{-1}) that tend to increase with height in layers of strong wind shear, particularly in the tropics and SH extratropics. Moreover, the Aeolus QC acts to retain HLOSV with larger uncertainties at levels above 200 hPa; this would explain the corresponding increase in total SDCD at those levels. To better isolate the AMV error, the Aeolus error estimate is removed from the total SDCD at each level, resulting in mean profiles of adjusted SDCD (long dashed lines in Figs. 7b, 7e, and 7h) that include AMV errors and collocation/representativeness errors. Overall, the adjusted SDCD for all AMV types exhibit similar magnitudes and distributions in each geographic region throughout the vertical. WVclear comparisons have slightly smaller adjusted SDCD at upper levels, suggesting that sampling differences may play a role in the higher accuracy observed for WVclear AMVs, given that WVclear representativeness errors are likely small due to Aeolus RAY and WVclear AMVs observing similar scenes. Aeolus RAY uncertainty is larger in the presence of clouds and appears to have a considerable impact on the corresponding SDCD, as the reductions in IR and WVcloud SDCD (~1 m s^{-1}) are larger than for WVclear SDCD (0.5 m s^{-1}). In the NH

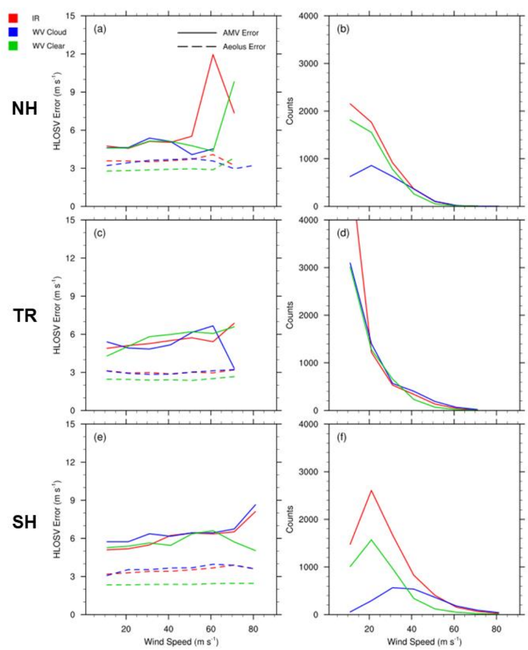

Figure 8: AMV HLOSV error (SDCD-Aeolus uncertainty) derived from GOES-16 RAY comparisons (solid lines) (m s^{-1}) and Aeolus L2B uncertainty (dashed lines) (m s^{-1}) with respect to AMV wind speed binned at 10 m s^{-1} for (a) NH, (b) tropics (TR), and (c) SH. (d-f) Counts per 10 m s^{-1} bin for each region.

Commented [KL30]: R2 specific point 17

extratropics, the adjusted SDCD for each AMV type is generally constant around 5 m s^{-1}, and in the tropics it increases with decreasing pressure from 5 to 6 m s^{-1}. AMV-RAY comparisons generally exhibit larger MCD and SDCD in the SH extratropics at upper levels due to the wind-shear height assignment error effect. This is illustrated in Fig. 8 that shows that the adjusted SDCD (solid lines) for all AMV types notably increase with increasing AMV wind speed in the SH extratropics relative to the other regions. This is also true for Aeolus error estimates (dashed lines) associated with IR and WVcloud comparisons in the SH (Fig. 8e).

(2002). SDCD are constant in the vertical around 6 m s^{-1} in the NH; SDCD in the SH are larger (6-8 m s^{-1}) and increase with height. Aeolus L2B uncertainty represents about half of the SDCD and is smallest for WVclear winds (2.5-3 m s^{-1}) and largest for IR and WVcloud winds (3-4 m s^{-1}) in all geographic regions. In the tropics, winds speeds peak in intensity around 300-400 hPa, suggesting enhanced wind shear within that layer. A small fast bias, that is the positive MCD of 0.5-1.0 m s^{-1}, could be due to height assignment errors in layers of high winds and enhanced vertical wind shear (Cotton et al. 2020). IR and WVcloud collocation counts in the tropics peak around 200 hPa and depict higher cloud-top motions related to the ITCZ, e.g., possibly thin anvil cirrus, which can hinder accurate height assignments to the AMVs. Moreover, the Aeolus QC acts to retain winds with larger uncertainties at levels above 200 hPa. This would explain the corresponding increase in SDCD at these levels. In all regions, WVclear AMVs exhibit smaller SDCD relative to the other channel types.

The findings confirm that QC'd GOES-16 AMVs exhibit relatively small MCD (with magnitudes less than 1.0 m s^{-1}) with respect to QC'd Aeolus RAY winds, with SDCD values (5-7 m s^{-1}) that are close to AMV error values relative to radiosondes/rawinsondes (see Table 1). AMV MCD and SDCD relative to Aeolus winds are found to be dependent on AMV method, geographic region, and vertical layer, in agreement with the findings in Velden et al. (1997) and Posselt et al., (2019). SDCD values tend to be larger in the SH extratropics where upper-level winds associated with the stronger subtropical jet storm track in winter are enhanced (Trenberth, 1991; Hoskins and Hodges, 2005). Among the three AMV methods examined, WVclear AMVs perform best with respect to Aeolus RAY winds and exhibit small yet significant HLOSV differences that generally match AMV performance metrics with respect to high quality radiosonde winds. Although we compare mean AMV-Aeolus collocation differences with speed statistics, it should be noted that in general, the HLOS wind generally approximates the zonal component of the horizontal flow (away from the poles) rather than the wind speed. However, the magnitude of the mean HLOS wind can act as a good approximation of the wind speed in regions where the mean flow is more zonal (e.g., away from the poles).

4.1.2 Mie-cloudy (MIE) comparisons

~~AMVs more closely match collocated MIE winds compared to RAY, due in part to smaller MIE random errors.~~ Figure ~~6~~9 presents density scatterplots ~~similar to~~like those in Fig. ~~4~~6 but compares ~~AMV and~~ GOES-16 AMVs and MIE winds. MIE SDCD are considerably smaller than those for RAY comparisons, and this is attributed to the general higher accuracy of Aeolus MIE ~~winds. Only~~ wind retrievals. Another possible reason is that MIE comparisons might generally have smaller collocation errors: because collocated Aeolus MIE winds and IR and WVcloud ~~AMV collocations are shown, as MIE winds represent~~AMVs are by definition more likely sampling similar cloudy scenes ~~and WVclear channels are tuned to track moisture features in clear skies.~~ at similar altitudes, we expect the Aeolus and AMV random and representativeness errors to be small (hereafter the cloudy/cloudy sampling effect). IR and WVcloud ~~winds correspond very well~~AMVs are highly correlated with MIE winds~~; the collocations exhibit high correlations,~~ ranging from 0.93 in the NH extratropics to 0.97 in the tropics. Most MIE collocations fall along the one-to-one line that corresponds to a perfect match. Statistics of AMV minus MIE collocation differences are generally consistent, albeit with some notable exceptions, with those for AMV comparisons with high-quality rawinsonde winds. MCD and SDCD are smallest in the tropics at -0.3 m s^{-1} and 4.4~~-~~ to 4.6 m s^{-1}, respectively, particularly for WVcloud comparisons which seem to have the fewest outliers. SH extratropical comparisons exhibit the largest SDCD (around 5~~-~~5.2 m s^{-1}) ~~which~~but are still ~~fall within range of~~ comparable to those associated with high~~-~~quality ~~radiosonde~~rawinsonde winds (Velden and Bedka, 2009; Santek et al., 2019). ~~Corresponding Aeolus L2B uncertainty represents almost 50% of the MIE SDCD and is generally constant (2 m s^{-1}), particularly at levels above 400 hPa, in all geographic regions. MIE comparison SDCD and L2B uncertainty are considerably~~

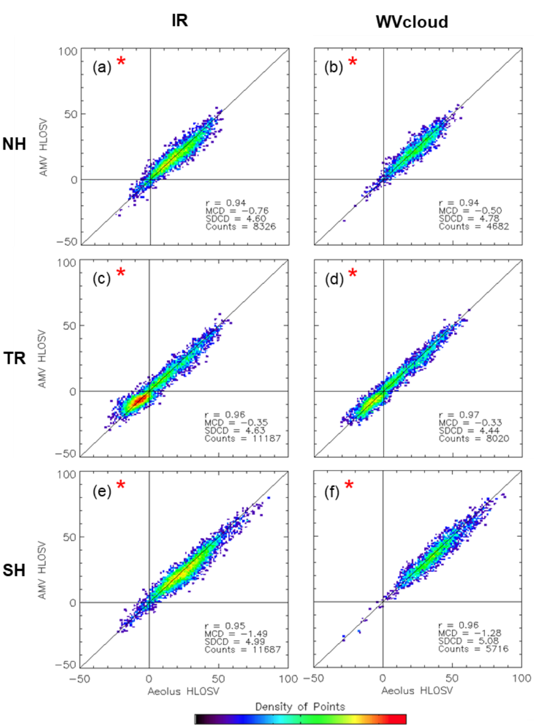

Figure 9: As in Fig. 6 but for comparisons of IR (left) and WVcloud (right) AMVs and MIE winds.

Formatted: Space Before: 6 pt

Formatted: TBD, Font color: Auto

Formatted: TBD, Font color: Auto

Commented [KL31]: R2 specific point 19

Commented [KL32]: R2 specific point 21

~~smaller than those for RAY comparisons, and this could be attributed to a combination of better correlated AMVs derived from motions in cloudy scenes and the higher accuracy of Aeolus MIE wind retrievals. The mean collocation distances for MIE winds (~51 km) is only slightly smaller than for RAY winds (~60 km) and should not contribute much to the smaller MIE SDCD.~~

The smaller SDCD observed in the NH and tropics suggest that AMVs accurately represent~~ well the~~ cloud-tracked motions associated with the North Atlantic storm track in summer and the summer-shifted ITCZ; such features are well-defined by high MIE number densities in the north and middle portions of the GOES-16 field-of-view in Fig. ~~1b~~4b. The larger SH SDCD suggest reduced accuracy in AMV winds that could be due to the wind-shear height assignment ~~errors in regions of higher wind speed and shear associated with stronger SH winter storm tracks~~error effect.

~~Figure~~ Similar to Fig. 7, Fig. 10 depicts ~~the~~ vertical distributions of AMV and MIE HLOSV and ~~the~~their differences ~~between AMV and MIE winds. Compared to the RAY collocations, the~~ . In the tropics and NH extratropics, MIE ~~collocations show virtually~~comparisons have nearly identical profiles of HLOSV ~~speeds~~ for the IR and WVcloud samples ~~but different vertical distributions of the differences as well as smaller SDCD in each geographic region. Significant negative MCD are~~ , with the largest ~~at -1.5 m s-1~~MCD observed at mid-levels in the tropics ~~and -2.0~~(at -1.5 m s^{-1}) and at upper-levels in the NH extratropics~~,~~ (-2.0 m s^{-1}), respectively. However, some of the larger differences occur at levels with a small sample size and may not be reliable. ~~In the tropics, the largest MCD correspond to winds~~ Despite the vertical variation of the MCD, profiles of total and adjusted SDCD are relatively constant at 4-5 m s^{-1}, and the contribution of Aeolus uncertainty to the total SDCD is small, as the removal of Aeolus errors only slightly reduces the SDCD. The results suggest that for MIE comparisons, the dominant factors contributing to the error consist of some combination of AMV random and representativeness/collocation error.

Formatted: Not Superscript/ Subscript

Formatted: Not Superscript/ Subscript

Commented [KL33]: R2 specific point 19

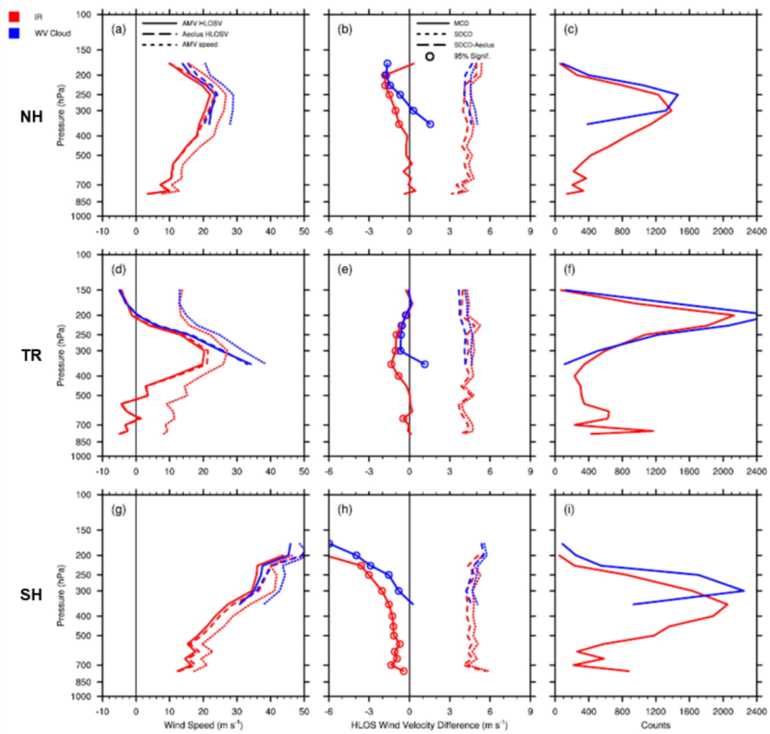

Figure 10: As in Fig. 7 but for comparisons of IR (red) and WVcloud (blue) AMVs and MIE winds.

In the NH above 250 hPa, SDCD increase slightly with decreasing pressure in a region of strong wind shear that could lead to larger AMV height assignment errors and representativeness errors. Indeed, the adjusted SDCD is shown to be larger for faster AMV wind speeds while the corresponding Aeolus MIE error estimates remain relatively constant (Fig. 11). This result in combination with likely small AMV-MIE collocation errors from the cloudy/cloudy sampling effect suggests that AMV height assignment errors dominate the larger SDCD observed in layers of high wind speed and strong shear. Additionally, in the tropics, a comparison with Aeolus MIE winds reveals a negative HLOSV bias in the IR and WVcloud GOES-16 AMVs below the higher cloud-tops of the ITCZ ~~and could~~ (Fig. 10e). Larger MCD appear at levels with higher wind speeds, as do larger values of adjusted SDCD, although the samples are small. Because Aeolus MIE errors remain small and constant around 2 m s^{-1} with respect to AMV wind speed (Fig. 11c), and AMV-MIE collocation errors are likely small, the results suggest that AMV height assignment errors contribute most to the negative MCD and corresponding larger SDCD, in agreement with Cotton et al. (2020, 2021) who also note a negative bias largely thought to be attributed to ~~height assignment errors combined with high winds and enhanced vertical wind shear in the region. Despite the vertical variation of the MCD, SDCD are relatively constant at 4-5 m s^{-1} in the tropics. In the NH extratropics, SDCD appear to slightly increase with height corresponding to AMV and Aeolus winds in regions of high wind speeds and enhanced wind shear.~~ AMV height assignment errors. This finding is relatively new, and the fact that comparisons with Aeolus depict this feature hints at the value of using Aeolus MIE winds as a standard for comparison to characterize cloud-tracked AMVs. Additionally, our comparisons with Aeolus depict another noted feature in monitoring AMVs by Cotton

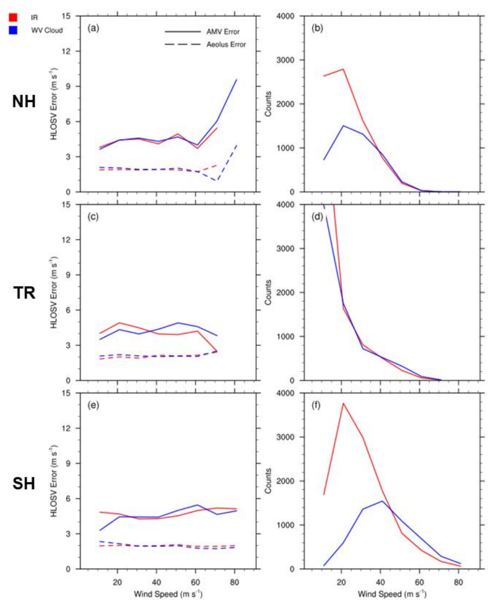

Figure 11: As in Fig. 8 but for MIE comparisons with GOES-16 IR (red) and WVcloud (blue) AMVs.

et al. (2020, 2021): a pronounced negative wind speed bias in the tropics for Meteosat-8 is evidenced by large negative MCD and correspond to large SDCD in all regions (not shown). This feature is evident in both RAY and MIE comparisons.

~~In~~MCD are largest in the SH extratropics~~,~~ and are statistically significant ~~HLOSV differences are relatively small~~ throughout the vertical, ranging from -1.0 m s^{-1} at low levels ~~(-1.0 m s^{-1}) and dramatically become more negative with height, reaching values that are more negative than~~to < -3.0 m s^{-1} above 300 hPa~~. It can be~~ (Fig. 10h). Strong wind shear corresponding to an intensified jet is inferred ~~that the high wind velocities at~~ at upper levels (Fig. ~~7g) exemplify an intensified jet and corresponding enhanced vertical wind shear in the region of the SH winter storm tracks. The large differences~~ 10g). The larger MCD aloft ~~exhibit relatively small~~ are associated with increases in adjusted SDCD with height, which are on the order of ~~5~~4-6 m s^{-1} ~~throughout the vertical. The larger mean differences~~. Moreover, the large MCD represent over 8.5% of the corresponding ~~high wind speeds~~ HLOSV at upper levels and could be attributed to larger AMV height assignment errors ~~in the region of~~ corresponding ~~enhanced vertical wind shear.~~

~~Statistics of AMV minus~~to stronger storm tracks in winter. This is exemplified in Fig. 11e where Aeolus MIE ~~collocation differences are consistent with those for AMV comparisons with high quality radiosonde winds. Good quality GOES-16 AMVs exhibit significant small MCD and SDCD in cloudy scenes. IR and WVcloud AMVs perform best in the tropics, and exhibit similar MCD and SDCD throughout the vertical in the tropics and NH extratropics. SDCD for MIE comparisons are considerably smaller than those for RAY winds, suggesting that RAY~~ errors are ~~greater than MIE errors, and in turn contribute more to the RAY SDCD than for MIE comparisons. MIE MCD exhibit unique behavior in the SH that highlights the known slow bias in the extratropical upper atmosphere. MCD in the SH extratropics are significant and large relative to the other geographic regions, and corresponding~~ shown to be small (2 m s^{-1}) and remain relatively constant with increasing AMV wind speed, while the adjusted SDCD are larger and increase with ~~height. The larger MCD and SDCD above~~

Formatted: Font color: Auto

Formatted: Not Superscript/ Subscript

Formatted: TBD, Font: 12 pt, Font color: Auto

Formatted: TBD, Font: 12 pt, Font color: Auto

Formatted: TBD, Font: 12 pt, Font color: Auto

300 hPa suggests that cloud-tracked upper-level motions are more difficult to quantify if they exist near levels of enhanced baroclinic instability, e.g., the extratropical SH winter storm tracks at jet stream level.AMV wind speeds > 40 m s^{-1}. The results

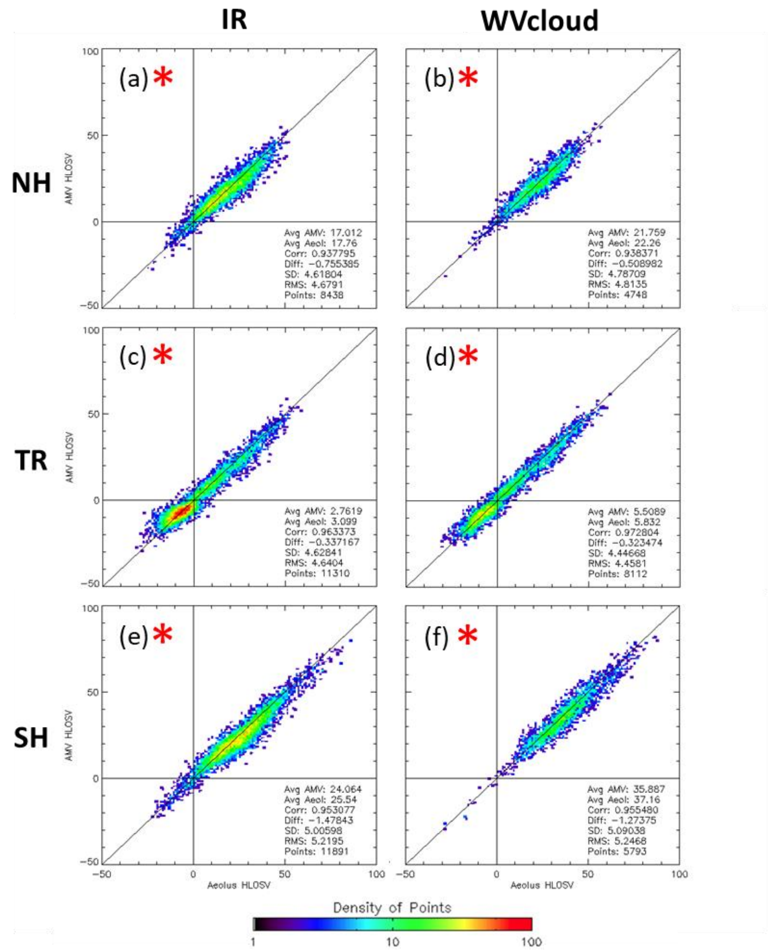

Figure 6: As in Figure 4 but for comparisons of IR (left) and WVcloud (right) AMVs and MIE winds.

imply that the large systematic differences in MCD at upper levels in the SH extratropics are most probably attributed to larger AMV errors in combination with strong wind shear.

Commented [KL34]: R2 specific point 20

760

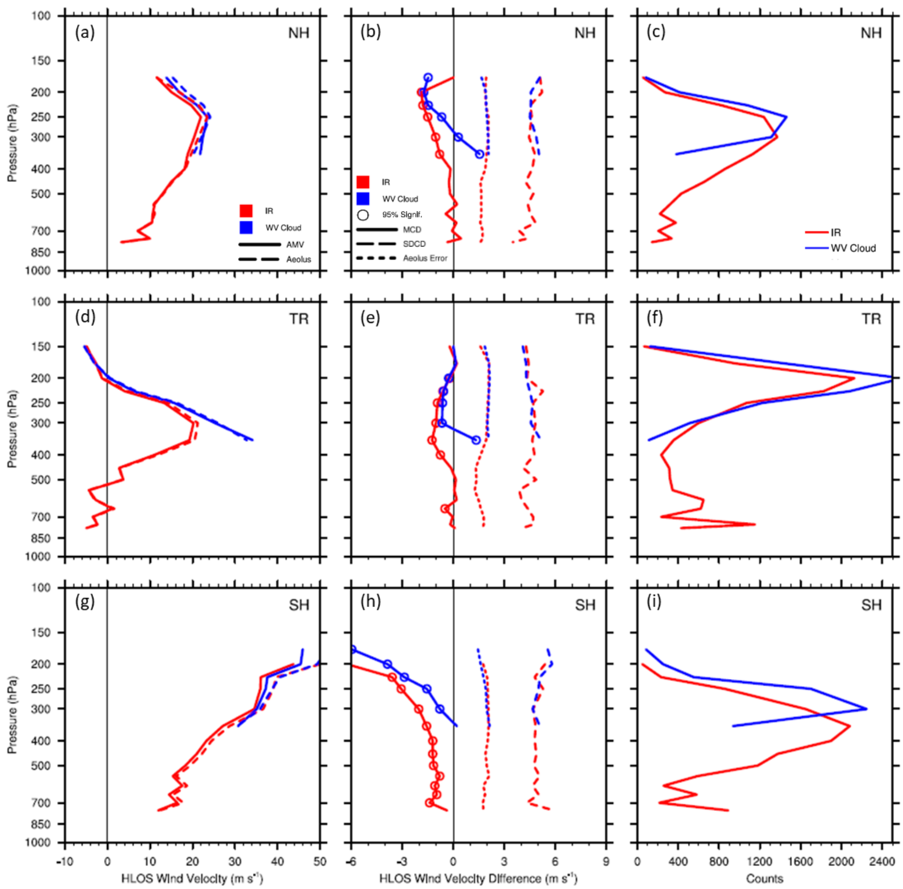

Figure 7: As in Figure 5 but for comparisons of IR (red) and WV cloud (blue) AMVs and MIE winds.

4.2 LEO AMVs vs. Aeolus

Formatted: Space Before: 6 pt

Figure 812 presents density scatterplots that compare LEO AMVs derived from IR window channels with RAY and MIE winds in the Arctic (Fig. 8a12a-b) and Antarctic polar regions (Fig. 8c12c-d).) during the study period. LEO AMVs correspond wellshow good correspondence with both Aeolus observing modes in the polar regions. Comparisons In general, comparisons in the Arctic have small yet significant mean differences in HLOSVMCD (around -0.2 m s^{-1}) and SDCD estimates of 5.2-6.5 m s^{-1}, while Antarctic comparisons exhibit larger MCD and SDCD. Further, Arctic Moreover, MIE comparisons in the Arctic exhibit the smallest SDCD, and Antarctic RAY comparisons in the Antarctic have the largest SDCD and more evident outliers. The results suggestThis suggests that during the study period of study in the Arctic, IR LEO AMVs are best able to capture cold scene cloud-tracked motions during the summer season (in the Arctic) when cloudiness increases in the vertical and more water vapor content is generally available to track features (Alekseev et al., 2018). Water vapor content in the Arctic is largest in summer due to an influx of water vapor from melting ice and snow and receding sea ice extent as well as enhancedintensified meridional moisture fluxes from low latitudes (Alexseev et al., 2018).

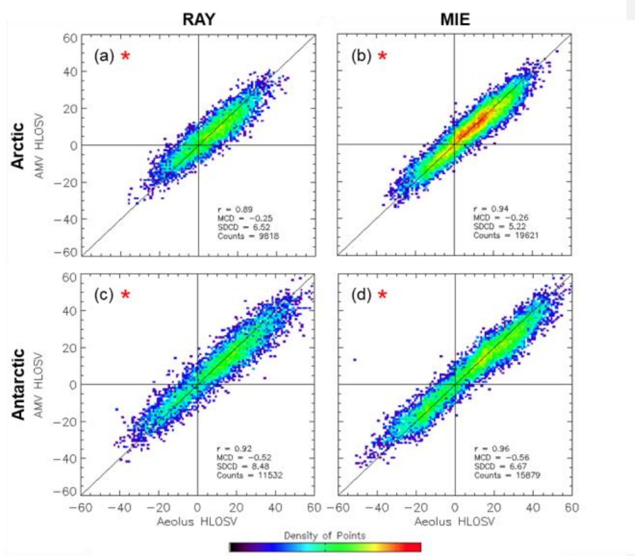

Figure 12: Density scatterplot of collocated IR-window AMVs from all available LEO satellites and RAY (left, a, c) and MIE (right, b, d) winds: Comparisons in (a-b) Arctic (north of 60° N), and (c-d) Antarctic (south of 60° S). Colors indicate total number of collocated observation pairs within the cells plotted, which are 1 ms^{-1} on a side. Sample statistics are displayed in the bottom right corner of each panel. Horizontal and vertical zero lines are plotted in black, as is the diagonal one-to-one line. Red star denotes statistical significance at the 95% level using the paired two-tailed Student's t-test. HLOSV units are m s^{-1}.

As was done for the GOES-16 case study, we examine the meanvertical differences in the vertical between all LEO AMV windsAMVs and Aeolus winds to ascertain how well AMVs characterize the dynamical flow at the poles (Fig. 913). RAY (red colors) and MIE comparisons (blue colors) comparisons are presented together. Figures 9a and 9d display the mean AMV AMV HLOSV and Aeolus HLOSV in the Arctic and Antarctic, respectively, and Fig. 9b and 9e show the MCD and SDCD. Corresponding observation countsprofiles are shown in Fig. 9c and 9f.

AMV and Aeolus winds exhibit similar speeds that increasethroughout the vertical, with height in both polar regions.notably larger MCD in the Antarctic at upper levels. In the Arctic (boreal summerFig. 13, top row), MIE winds and collocated AMVs showdepict faster motions relative to RAY comparisons in mid- to upper-levels.. Statistically significant MCD are on the order of -0.5 m s^{-1} at mid-levels where collocation counts peak, representing slower AMV winds relative to Aeolus. The mean differencesMCD become larger (more negative) nearer the tropopause (~(around 300-250 hPa) where speedsHLOSV reach upwards of 15 m s^{-1}. and AMV wind speeds reach 30 m s^{-1}, while corresponding total SDCD in the Arctic are relativelygenerally constant throughout the troposphere withbut smaller for MIE SDCD (~5 m s^{-1}) andthan RAY (~7 m s^{-1}). Removal of the Aeolus L2B uncertainty (1-2 m s^{-1}) relative to RAY (~7 m s^{-1} and 3-4 m s^{-1}, respectively), suggestingyields adjusted SDCD profiles that are nearly equal to the total MIE SDCD, indicating the higher accuracy of MIE winds. The in the Arctic at all levels including those with higher wind speeds. This independence of Aeolus MIE uncertainty to changes in wind speed is clear in Fig. 14a where Aeolus MIE errors are shown to be smaller relative to RAY and remain relatively constant with increasing AMV wind speeds. In addition, the near doubling of MIE collocation counts at mid-levels relative to RAY (Fig. 13c) could be due to increased cloudiness associated with more moisture availability in Arctic summer (Alekseev et al., 2018).

In the Antarctic (austral winter), wind speeds increase from 5 m s^{-1} at mid-levels to nearly 30 m s^{-1} at very high levels (~150 hPa), and RAY comparisons are shown to capture generally faster motions throughout the vertical column. MCD are small (around -0.5 m s^{-1}) at levels where collocation counts peak and become larger aloft in the layer of sharply increasing winds where they represent over 10% of the corresponding wind speeds. As in the Arctic, MIE comparisons in the Antarctic have smaller SDCD (6-7 m s^{-1}) and L2B uncertainty (2 m s^{-1}) than RAY (8-12 m s^{-1} and 4-5 m s^{-1}, respectively) throughout the vertical, but both exhibit larger uncertainties in the Antarctic. Further, RAY SDCD increase with height from ~7 m s^{-1} at low levels to over 10 m s^{-1} at very high altitudes; similarly, corresponding Aeolus RAY L2B uncertainties increase from 4-5 m s^{-1}. Larger MCD aloft in the Antarctic could be attributed to the lower accuracy of AMV height assignments in the layer of increasing wind speed and corresponding enhanced vertical wind shear related to the strengthening of the Antarctic polar vortex in late winter/early spring. Higher SDCD values at upper levels may be attributed to the inclusion of Aeolus winds with larger uncertainties above 200 hPa following the QC as well surface effects, as very cold brightness temperatures near the surface may be misinterpreted as high clouds (Key et al., 2016).

The relationship of LEO IR AMVs to Aeolus winds depends on the polar region and Aeolus observing mode, Rayleigh or Mie. Overall, polar AMVs have smaller MCD relative to MIE than RAY. In Arctic summer, more water vapor is available to track features throughout the vertical column, and this results in similar MCD and SDCD with respect to both Aeolus observing modes. Differences are small and significant for MIE comparisons, and SDCD are generally smaller than for RAY comparisons by 1-2 m s^{-1}. In Antarctic winter, MCD and SDCD become larger with height. This behavior may be partially due to the mischaracterization of cold surfaces as clouds and partially due to strong wind shear aloft related to a strengthening of the

Antarctic polar vortex, which would diminish the representativeness of AMVs and Aeolus winds as well as reduce the accuracy of corresponding height assignments.

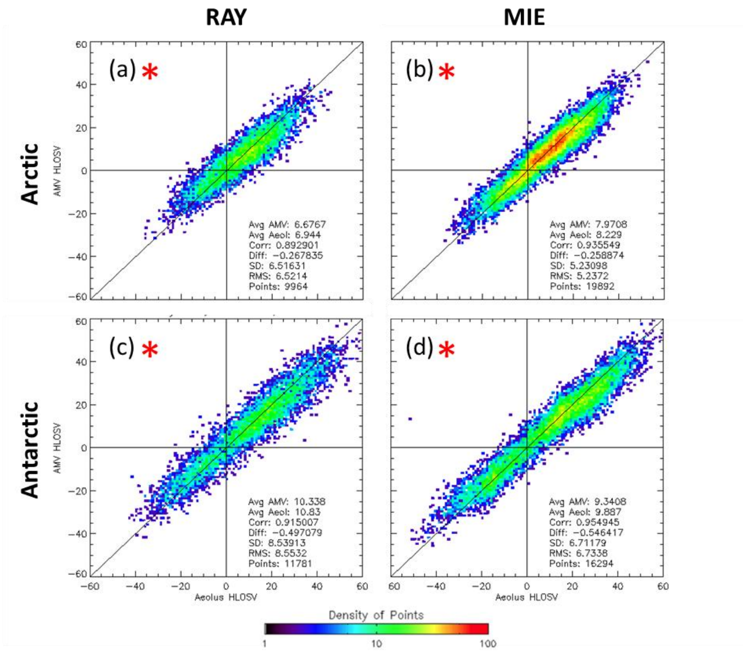

Figure 8: Density scatterplot of collocated IR-window AMVs from all available LEO satellites and RAY (left column) and MIE (right column) winds: Comparisons in (a-b) Arctic (north of 60° N), and (c-d) Antarctic (south of 60° S). Colors indicate total number of collocated observation pairs within the cells plotted, which are 1 ms^{-1} on a side. Sample statistics are displayed in the bottom right corner of each panel. Horizontal and vertical zero lines are plotted in black, as is the diagonal one-to-one line. Red star denotes statistical significance at the 95% level using the paired two-tailed Student's t-test. HLOSV units are $m\ s^{-1}$.

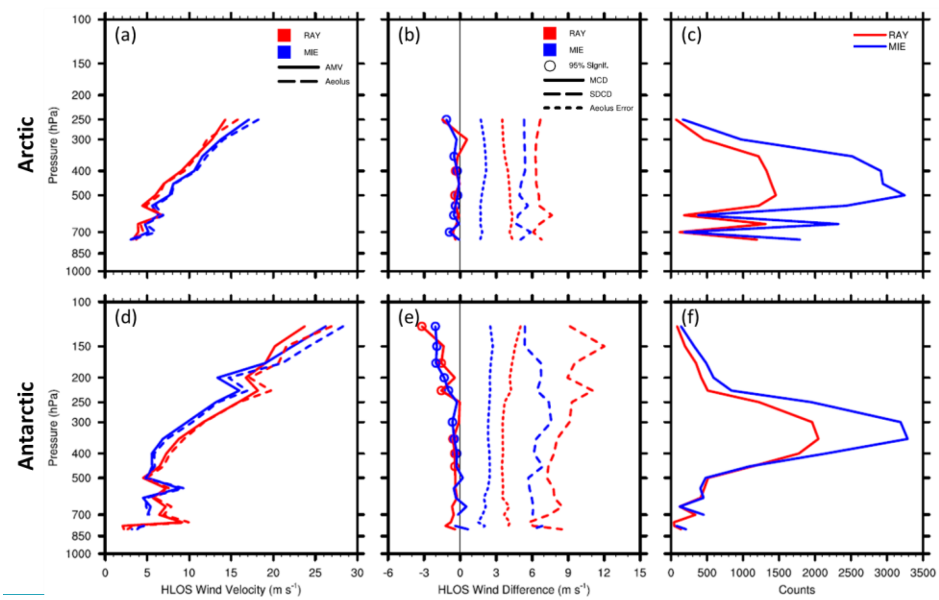
(a)
(b)
(c)
(d)
(e)
(f)
RAY
MIE
AMV
Aeolus
95% Signif.
MCD
SDCD
Aeolus Error
Arctic
Antarctic
Pressure (hPa)
HLOS Wind Velocity (m s-1)
HLOS Wind Difference (m s-1)
Counts

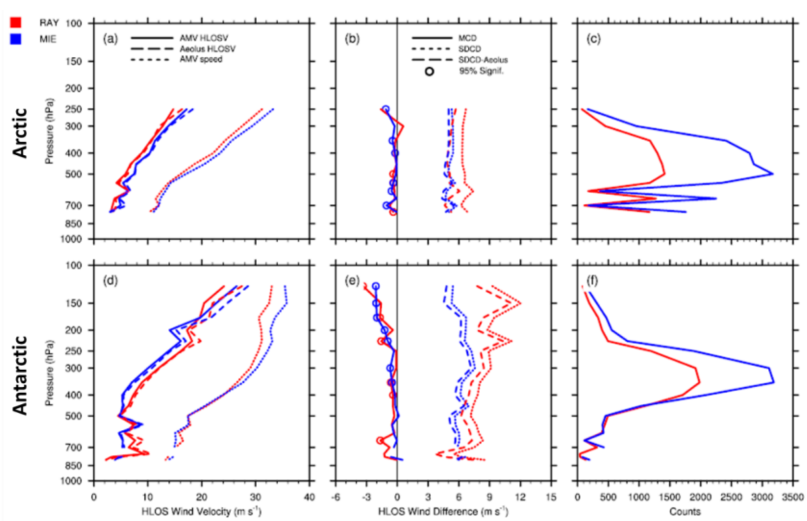
RAY
MIE
(a)
(b)
(c)
(d)
(e)
(f)
AMV HLOSV
Aeolus HLOSV
AMV speed
MCD
SDCD
SDCD-Aeolus
95% Signif.
Arctic
Antarctic
Pressure (hPa)
HLOS Wind Velocity (m s-1)
HLOS Wind Difference (m s-1)
Counts

Figure 13: Vertical ~~comparisons~~profiles of collocated LEO AMVs and RAY (red) and MIE (blue) winds. The top row shows the Arctic (north of 60° N), (a) mean AMV HLOSV (solid lines~~) and~~), Aeolus ~~(~~HLOSV (long dashed lines) ~~winds~~ (m s^{-1}), and mean AMV wind speed (short dashed lines) (m s^{-1}); (b) MCD (solid), SDCD (~~long~~short dashed), and AMV HLOSV error as represented by SDCD-Aeolus L2B uncertainty (~~short~~long dashed) (m s^{-1}~~),~~); and (c) collocation counts. (d-f) as in (a-c) but for the Antarctic (south of 60° S). Colored open circles indicate levels where MCD are statistically significant at the 95% level (p-value < 0.05) using the paired Student's *t*-test. Vertical zero lines are displayed in the center panels in black. Levels with observation counts > 25 are plotted.

In the Antarctic (Fig. 13, bottom row), HLOSV increase from 5 m s^{-1} at mid-levels to nearly 30 m s^{-1} at very high levels (~150 hPa), and RAY comparisons are shown to capture generally faster motions throughout much of the vertical column. MCD are small (around -0.5 m s^{-1}) at mid-levels where collocation counts peak but are larger aloft and represent over 10% of the corresponding HLOSV. Larger MCD aloft could be attributed to the wind-shear height assignment error effect related to the strengthening of the Antarctic polar vortex in late winter/early spring. As shown in the Arctic, MIE comparisons in the Antarctic have smaller total SDCD (5-7 m s^{-1}) than RAY (6-12 m s^{-1}, respectively) throughout the vertical; however, Antarctic MIE and RAY SDCD are larger than in the Arctic and appear to increase with height. Higher SDCD values at upper levels may be attributed to larger AMV and Aeolus errors in layers of faster winds. Adjusted SDCD as well as Aeolus error estimates for RAY comparisons increase with increasing AMV wind speed (Fig. 14c), suggesting that both AMV errors and Aeolus errors in layers of high winds and strong shear contribute to the larger SDCD observed in the Antarctic.

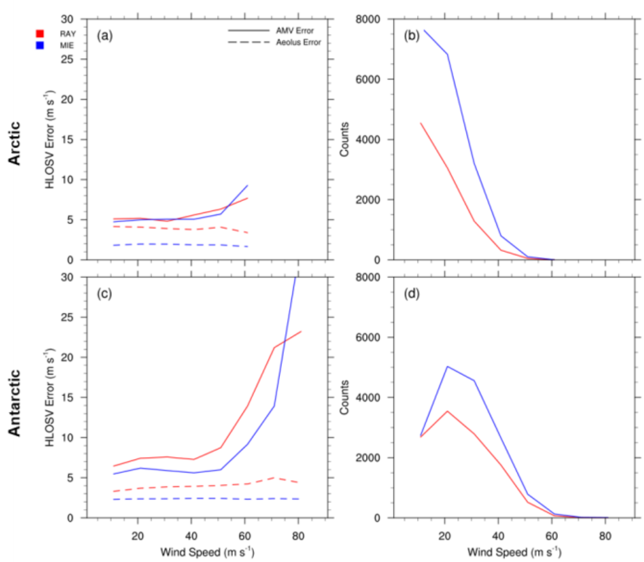

Figure 14: As in Fig. 8 but for LEO IR RAY and MIE comparisons at the poles.

5 Summary and conclusions

This study summarizes statistical comparisons of AMVs with the novel Aeolus L2B HLOS winds ~~based on~~for samples stratified by specific sets of conditions and discusses their relationship to known AMV characteristics. Because Aeolus observes the HLOSV—the horizontal wind projected onto the HLOS of the DWL—derived from the detection of molecular

Formatted: Font: Italic

Formatted: Font: 10 pt

Formatted: Space Before: 12 pt

and aerosol backscattering signals, the assessments of mean collocation differences (AMV minus Aeolus) and SD of the differences ~~(MCD and SDCD)~~ are all in terms of AMV winds projected onto the collocated Aeolus HLOS. In the tropics, due to the Aeolus observing geometry, HLOSV represents the zonal wind. Aeolus HLOSV profiles utilized in this study are classified as RAY or Rayleigh-clear winds (representing mostly clear-sky scenes) and MIE or Mie-cloudy winds (representing cloudy scenes only). ~~Quality controls recommended~~Winds quality controlled (QC'd) following recommendations by ESA for Aeolus and by the user community for the satellite winds are ~~applied. Quality controlled winds from each dataset are~~ retained for analysis.

The performance of ~~quality controlled~~ QC'd AMVs relative to collocated QC'd Aeolus winds ~~of quality controlled~~ are characterized by analyzing ~~the~~ sample statistics of the collocated differences, AMV HLOSV minus Aeolus HLOSV. These statistics should not be strictly interpreted as overall AMV performance, as differences arise from errors in both AMVs and Aeolus winds and from representativeness and collocation errors.

Comparisons of GOES-16 AMVs and IR ~~window~~ cloud-~~track~~tracked AMVs from LEO satellites are assessed to estimate the dependence of AMVs on different combinations of conditions including Aeolus observing mode/scene type (clear or cloudy), AMV ~~derivation method~~type (IR~~ window~~, WVcloud, and WVclear), and geographic region (tropics and extratropics for GOES-16, Arctic and Antarctic polar regions for LEO).~~ Vertical distributions of differences in HLOSV are examined, as this perspective has the potential to provide additional insight into how well each band for AMV retrievals represents the horizontal flow in the vertical.~~

~~Relative to Aeolus, AMV performance metrics exhibit different characteristics in clear and cloudy scenes that vary with geographic region and in the vertical, in agreement with the findings in Velden et al. (1997) and Posselt et al. (2019). Overall, GEO and LEO AMVs are found to correspond very well with Aeolus RAY and MIE winds, and on average GEO AMV minus Aeolus MCD and SDCD values fall within the ranges of known biases and uncertainties of AMVs. MCD are small, and SDCD and mean collocation distances are smaller for MIE compared to RAY collocations, reflecting the higher accuracy of MIE winds and of AMVs in cloudy scenes and possibly larger collocation errors for the RAY winds which tend to have larger collocation distances with AMVs relative to MIE. Larger SDCD are evident in the SH where wind shear is enhanced especially in winter due to the strengthening of the Antarctic polar vortex (Zuev and Savelieva, 2019), which can affect the representativeness of both AMVs and Aeolus winds. In the Arctic, MIE comparisons exhibit small MCD and SDCD consistent with known LEO AMV characteristics, while Antarctic RAY and MIE comparisons show generally larger SDCD.~~

~~GOES-16 and LEO AMV MCD and SDCD characterizations based on Aeolus winds are summarized.~~ GOES-16 was chosen as a representative of GEO performance, as the AMVs exhibit high correlations with Aeolus, relatively low MCD and SDCD, and have a large sample size from which to compute robust statistics. The summary assessment of all LEO AMVs provides a unique, comprehensive perspective on the characteristics of polar AMVs using a larger sample of collocated Aeolus wind profiles relative to other available datasets, e.g., ~~radiosonde profile data~~rawinsonde profile data. Vertical distributions of differences in HLOSV are examined, as this perspective has the potential to provide additional insight into how accurately each AMV type represents the horizontal flow in the vertical. AMVs exhibit different characteristics in clear and cloudy scenes that vary with geographic region and in the vertical, in agreement with the findings in Velden et al. (1997), Posselt et al. (2019), and others. Overall, GEO and LEO AMVs are found to compare as well with Aeolus RAY and MIE winds as they do to conventional data sources and NWP products, particularly in the tropics, NH extratropics, in the Arctic, and at mid- to upper-levels in both clear and cloudy scenes. SH comparisons generally exhibit larger than expected SDCD that could be attributed to larger height assignment errors and larger representativeness and collocation errors in regions of high winds and strong vertical wind shear.

GOES-16 AMVs are found to correspond well with RAY and MIE winds. In clear scenes in the tropics and NH extratropics, MCD are small and SDCD fall within the accepted range of AMV error values when compared with high quality radiosonde winds (Velden and Bedka, 2009; Santek et al., 2019). WVclear AMVs perform best with respect to Aeolus RAY winds, with smaller MCD (-0.6 m s^{-1} to 0.3 m s^{-1}) and SDCD values (5.4-5.6 m s^{-1}) relative to other AMV channel types. Relative to MIE winds, IR window cloud-track and WVcloud AMVs exhibit similar MCD in the tropics (-0.3 m s^{-1}) and NH extratropics (-0.5 m s^{-1} to -0.7 m s^{-1}), with WVcloud AMVs exhibiting the smallest SDCD. MIE collocations have smaller SDCD (~4.4 m s^{-1} to 4.8 m s^{-1}) and corresponding Aeolus L2B uncertainty (1-2 m s^{-1}) than RAY collocations. In the SH extratropics, MCD are large relative to the other geographic regions, and SDCD estimates are larger and increase with height, suggesting that cloud- and moisture-tracked motions related to extratropical SH winter storm tracks may be more difficult to accurately quantify in the SH, particularly near the jet stream level.

The relation of LEO IR AMVs to Aeolus winds differs between RAY and MIE comparisons (i.e., in clear vs cloudy scenes) and varies with polar region and Aeolus observing mode. Overall, MIE comparisons have smaller MCD compared to RAY. In Arctic summer, MIE MCD are small but statistically significant, and SDCD and corresponding Aeolus L2B uncertainties are generally smaller than for RAY collocations by 1-2 m s^{-1}. In Antarctic winter, mean AMV and Aeolus winds sharply increase with height. The corresponding MCD become more negative and SDCD are larger than in the Arctic and also increase with height. The larger MCD aloft could be attributed to the lower accuracy of AMV height assignments in regions of high winds and strong wind shear related to the strengthening of the Antarctic polar vortex in late winter/early spring, as well as the possible mischaracterization of very cold surface temperatures as clouds. The inclusion of Aeolus winds with larger uncertainties above 200 hPa may also play a role.

The findings presented here provide information on the variation of AMV characteristics relative to Aeolus RAY and MIE winds, and suggest that Aeolus could be used as a standard for the comparative assessment of AMVs pending additional bias corrections to the Aeolus L2B winds. Comparisons with Aeolus HLOS winds provide estimates consistent with known AMV bias and uncertainty in the tropics, NH extratropics, and in the Arctic, and at mid- to upper-levels in both clear and cloudy scenes. WVclear winds perform best relative to RAY winds. Comparisons between IR and WVcloud AMVs and Aeolus MIE winds reveal similar MCD and significant smaller SDCD in the NH and tropics with respect to RAY comparisons. SH comparisons generally exhibit larger SDCD that could be attributed to height assignment errors in regions of high winds and

Commented [KL35]: R2 main point 2, specific point 22

Formatted: Font: Not Bold

~~enhanced vertical wind shear. The level of agreement between AMVs and Aeolus winds varies per stratification including the Aeolus observing mode coupled with AMV derivation method, geographic region, and height of the collocated winds. These combinations of conditions should be considered in future comparison studies and impact assessments involving 3D winds. Additional corrections to the Aeolus dataset, e.g., via the removal of DWL instrument calibration-dependent error or a bias correction utilizing Total Least Squares regression as discussed in Liu, H. et al. (2021), are anticipated to further refine the results.~~

~~The use of Aeolus HLOS winds as a benchmark dataset has valuable implications for future endeavors involving validation of 3D winds and the use of such data in NWP. For example, these findings~~The main findings from comparing GOES-16 AMVs with RAY and MIE winds are the following. Aeolus MIE winds show great potential value as a comparison standard to characterize AMVs. MIE comparisons generally exhibit smaller biases and uncertainties compared to RAY, reflecting the higher accuracy of MIE winds and AMVs in cloudy scenes as well as larger collocation errors for RAY winds in cloudy scenes. This is attributed to a combination of smaller Aeolus MIE uncertainties and smaller collocation/representativeness errors due to the cloudy/cloudy sampling effect, that is, the fact that both Aeolus and AMV winds are, by definition, sampling similar cloudy scenes at similar altitudes. The contribution of Aeolus MIE uncertainty to the overall SDCD is small; in fact, removal of Aeolus uncertainties further reduces the small MIE SDCD without much change to its vertical distribution, suggesting that for MIE comparisons, the dominant factors contributing to the total error consist of AMV random errors and representativeness/collocation errors. Additionally, the AMV-Aeolus MIE comparisons depict a relatively new finding that is also noted in Cotton et al. (2020, 2021) and is largely thought to be attributed to AMV height assignment errors: a negative speed bias in the IR and WVcloud AMVs in the tropics. The fact that comparisons with Aeolus exhibit this feature hints at the usefulness of Aeolus MIE winds as a standard for comparison to characterize AMVs. (It should be noted that because the period of study is relatively short, the datasets are not large enough to examine in detail many of the "features" identified and studied in the NWP SAF AMV monitoring. However, it could be possible to verify the identification of such features in AMV comparisons with Aeolus observations by using a larger collocation dataset, which the authors are preparing and making publicly available.)

Regarding GOES-16 RAY comparisons, sampling differences may play a role in the higher correlation between Aeolus RAY winds and WVclear AMVs, since they both represent similar clear-sky scenes. This is especially true in the tropics and NH extratropics where MCD are small and SDCD are comparable to AMV error values compared with high-quality rawinsonde winds. It is likely that collocation errors play a larger role in the RAY SDCD for IR and WVcloud AMVs due to the cloudy/clear sampling effect, where clear-sky Aeolus winds are collocated with cloudy AMVs and thereby observe different scenes, yielding larger errors. In addition, the removal of Aeolus uncertainties from the total SDCD considerably reduces the RAY SDCD, particularly for IR and WVcloud comparisons, indicating that Aeolus contributes a substantial fraction of the total SDCD in the presence of clouds.

Commented [KL36]: R2 specific point 23

Commented [KL37]: R2 specific point 19

Commented [KL38]: R2 specific point 17

Polar AMVs have smaller MCD for MIE compared to RAY, although Antarctic AMVs have larger SDCD than the Arctic. In fact, GEO and LEO comparisons in the SH/Antarctic exhibit the largest SDCD of all regions examined. Large wind shear is evident in the SH/Antarctic throughout much of the atmospheric column, and this can dramatically affect AMV height assignment errors. Indeed, AMV errors are shown to generally increase with increasing AMV wind speed, as do corresponding Aeolus errors for RAY winds, suggesting that both contribute to the larger SDCD observed in layers of high wind speed. Additionally, larger RAY MCD aloft could be attributed to larger collocation/representativeness errors due to IR AMVs and RAY winds viewing different scenes. The possible mischaracterization of very cold surface temperatures as clouds may also be a factor. For GOES-16 MIE comparisons in the SH, AMV errors are larger and increase with AMV speeds > 40 m s^{-1} while Aeolus MIE errors are small and remain relatively constant. This implies that the large systematic differences in MCD at upper levels in the SH extratropics are most probably attributed to larger AMV errors in combination with the wind-shear height assignment error effect.

The use of Aeolus winds as a benchmark dataset for the comparative assessment of AMVs has valuable implications for future research, including the validation of 3D winds and the use of such data in NWP. For example, the findings presented here contribute to the ongoing development of a feature track correction (FTC) observation operator to account for AMV height assignment and other biases in data assimilation (Hoffman et al., ~~2021~~2022). One lesson learned from this study is that QC of both AMV and Aeolus observations is critical and largely improves the results. The Aeolus project has done much to eliminate errors of all types, but some improvements are expected, e.g., via the removal of DWL instrument calibration-dependent error. Further, some of the bias corrections currently applied depend on ECMWF forecasts, and the analysis of Liu et al. (2022) demonstrates that additional bias corrections for Aeolus are possible, and that such corrections can improve NWP analysis and forecast results (Garrett et al., 2022).

Appendix A

Formulae for the statistics used in this study are presented here. Since HLOSV is a scalar, these formulae correspond directly with the standard textbook formulae. The collocation database is composed of pairs (x_i, y_i) for i=1, n, where n is the number of collocations, i is the collocation index, x is the Aeolus HLOSV, and y is the AMV HLOSV. The correlation (r) between collocated HLOSV describes the overall relation of AMVs to Aeolus and is defined as

$$r = \frac{\sum_{i=1}^{n}(x_i-\bar{x})(y_i-\bar{y})}{s_x s_y} \qquad \text{(A1)}$$

Overbars denote sample means. The corresponding standard deviations s_x and s_y are defined as

$$s_m \equiv \sqrt{\frac{1}{n-1}\sum_{i=1}^{n}(w_i-\bar{w})^2} \qquad \text{(A2)}$$

Commented [KL39]: R2 main point 1

Commented [RH40]: I don't know. Would require height assignments to be in the same direction (high or low) to generate large MCDs.
Fig.10h indicates all the assigned heights are too high.
But then why just mostly for MIE.

Formatted: BodyText, Justified, Line spacing: 1.5 lines

Formatted: Font: 10 pt

Formatted: Font: 10 pt

Commented [KL41]: R2 specific comment 25

Commented [KL42]: R1 point 1

where w can equal x or y. The collocation difference (CD) is the difference in m s^{-1} between each pair of collocated AMV HLOSV and Aeolus HLOSV,

$$CD = y_i - x_i \qquad \text{(A3)}$$

and the mean (MCD) represents the sample mean of the CD for select conditions, such as a specific geographic region, pressure level, AMV type, or Aeolus observing mode.

$$MCD = \frac{1}{n}\sum_{i=1}^{n}(CD) \qquad \text{(A4)}$$

Using (A2), we can define the corresponding SDCD in terms of CD:

$$SDCD = \sqrt{\frac{1}{n-1}\sum_{i=1}^{n}(CD_i - MCD)^2} \qquad \text{(A5)}$$

Finally, the "adjusted SDCD" s_{adj} is defined as the SDCD with the corresponding Aeolus error estimate s_x removed:

$$s_{adj} = \sqrt{SDCD^2 - s_x^2} \qquad \text{(A6)}$$

Data availability

Formatted: Space Before: 12 pt

The Aeolus L2B Earth Explorer data used in this study are publicly available and can be accessed via the ESA Aeolus Online Dissemination System (https://aeolus-ds.eo.esa.int/oads/access/). The NCEP SATWND BUFR AMV dataset can be provided by the corresponding author (katherine.lukens@noaa.gov) upon request. Additionally, the authors are preparing an Aeolus-AMV collocation dataset that will be provided upon request.

Author contributions

Formatted: Space Before: 12 pt

Kevin Garrett and Kayo Ide proposed the project as co-investigators and provided expertise that guided this work. Brett Hoover and David Santek developed the collocation algorithm used. Katherine E. Lukens performed most of the work that included the implementation of the collocation algorithm and comparison analysis. David Santek and Ross N. Hoffman provided additional intellectual support that considerably improved the article. Katherine E. Lukens prepared the manuscript with contributions from all co-authors.

Competing interests

Formatted: Space Before: 12 pt

The authors declare that they have no conflict of interest.

Acknowledgements

The authors would like tothank the two anonymous referees for their careful and helpful comments that considerably improved the article. The authors also thank their colleagues at NOAA/NESDIS/STAR for overseeing this work as well as Dr. Mike Hardesty of CSU/CIRA, Dr., Iliana Genkova of IM Systems Group, Inc. (IMSG),, and the rest of the US Aeolus Cal/Val team for guidance and support. The University of Wisconsin-Madison S4 supercomputing system (Boukabara et al., 2016) was used in this work. The authors acknowledge support from the NOAA/NESDIS Office of Projects, Planning, and Acquisition (OPPA) Technology Maturation Program (TMP) through CICS and CISESS at the University of Maryland/ESSIC [NA14NES4320003 and NA19NES4320002] and CIMSS at the University of Wisconsin-Madison [NA20NES4320003]. The scientific results and conclusions, as well as any views or opinions expressed herein, are those of the authors and do not necessarily reflect those of NOAA or the U.S. Department of Commerce.

Formatted: Space Before: 12 pt

References

Formatted: Space Before: 12 pt

Formatted: Font: Times New Roman

Abdalla, S., de Kloe, J., Flament, T., Krisch, I., Marksteiner, U., Reitebuch, O., Rennie, M., Weiler, F., and Witschas, B.: Verification report of first Reprocessing campaign for FM-B covering the time period 2019-06 to 2019-12. Tech. rep., Aeolus Data Innovation Science Cluster DISC, Version 1.0, REF: AED-TN-ECMWF-GEN-040, internal document available for registered Aeolus Cal/Val teams; Summary of this document available at: https://earth.esa.int/eogateway/documents/20142/0/Aeolus-Summary-Reprocessing-1-DISC.pdf, 2020.

Alekseev, G., Kuzmina, S., Bobylev, L., Urazgildeeva, A., and Gnatiuk, N.: Impact of atmospheric heat and moisture transport on the Arctic warming. Int. J. Climatol., 39, 3582–3592, doi:10.1002/joc.6040, 2018.

Bedka, K. M., Velden, C. S. Petersen, R. A. Feltz, W. F., and Mecikalski, J. R.: Comparisons of Satellite-Derived Atmospheric Motion Vectors, Rawinsondes, and NOAA Wind Profiler Observations. J. Applied Meteor. Clim., 48, 1542-1561, doi: 10.1175/2009JAMC1867.1, 2009.

Berger, H., Langland, R., Velden, C. S., Reynolds, C. A., and Pauley, P. M.: Impact of enhanced satellite-derived atmospheric motion vector observations on numerical tropical cyclone track forecasts in the western North Pacific during TPARC/TCS-08. J. Appl. Meteor. Climatol., 50, 2309–2318, doi:10.1175/JAMC-D-11-019.1, 2011.

Bormann, N., Kelly, G., and Thépaut, J.-N.: Characterising and correcting speed biases in atmospheric motion vectors within the ECMWF system. In Sixth Int. Winds Workshop, Madison, WI, EUMETSAT, 113–120. Available online at http://cimss.ssec.wisc.edu/iwwg/iww6/session3/bormann_1_bias.pdf, 2002.

Bormann, N., Saarinen, S., Kelly, G., and Thepaut, J.-N.: The Spatial Structure of Observation Errors in Atmospheric Motion Vectors from Geostationary Satellite Data. Mon. Wea. Rev., 131, 706-718, doi:10.1175/1520-0493(2003)131<0706:TSSOOE>2.0.CO;2, 2003.

Boukabara, S. A., Zhu, T., Tolman, H. L., Lord, S., Goodman, S., Atlas, R., Goldberg, M., Auligne, T., Pierce, B., Cucurull, L., Zupanski, M., Zhang, M., Moradi, I., Otkin, J., Santek, D., Hoover, B., Pu, Z., Zhan, X., Hain, C., Kalnay, E., Hotta, D., Nolin, S., Bayler, E., Mehra, A., Casey, S. P. F., Lindsey, D., Grasso, L., Kumar, V. K., Powell, A., Xu, J., Greenwald, T., Zajic, J., Li, J., Li, J., Li, B., Liu, J., Fang, L., Wang, P., and Chen, T.-C.: S4: An O2R/R2O infrastructure for optimizing satellite data utilization in NOAA numerical modeling systems. a step toward bridging the gap between research and operations. Bull. Amer. Meteor. Soc., 97, 2359–2378, doi:10.1175/bams-d-14-00188.1, 2016.

Bresky, W. C., Daniels, J. M., Bailey, A. A., and Wanzong, S.T.: New methods towards minimizing the slow speed bias associated with atmospheric motion vectors, *J.* Appl. Meteorol. Climatol., 51, 2137–2151, doi:10.1175/JAMC-D-11-0234.1, 2012.

Chen, S., Cao, R., Xie, Y., Zhang, Y., Tan, W., Chen, H., Guo, P., and Zhao, P.: Study on the seasonal variation of Aeolus detection performance over China using ERA5 and radiosonde data. Atmos. Chem. Phys. Discuss., https://doi.org/10.5194/acp-2021-298, 2021.

Cordoba, M., Dance, S. L., Kelly, G. A., Nichols, N. K., and Walker, J. A.: Diagnosing atmospheric motion vector observation errors for an operational high-resolution data assimilation system. Q. J. R. Meteorol. Soc., 143: 333–341, doi:10.1002/qj.2925, 2017.

Cotton, J., Doherty, A., Lean, K., Forsythe, M., and Cress, A.: NWP SAF AMV monitoring: the 9th Analysis Report (AR9). Tech. rep., NWP SAF, Version 1.0, REF: NWPSAF-MO-TR-039. Available at: https://nwpsaf.eu/monitoring/amv/nwpsaf_mo_tr_029.pdf,Available at: https://nwp-saf.eumetsat.int/site/monitoring/winds-quality-evaluation/amv/amv-analysis-reports/, 2020.

Cotton, J., A. Doherty, and K. Lean: Characterising AMV errors using the NWP SAF monitoring. In 15th IWWG Workshop. Available online at https://www.ssec.wisc.edu/meetings/iwwg/2021-meeting/presentations/oral-cotton/, 2021.

Cress, A.: Validation and impact assessment of Aeolus observations in the DWD modelling system Status report. In Aeolus NWP impact working meeting 2, Virtual. Available online at https://www.aeolus.esa.int/confluence/display/CALVAL/Aeolus+NWP+impact+working+meeting+2?preview=/12354328/12354463/5_DWD_acress_aeolus_20200617.pdf, 2020.

Daniels, J., Bresky, W., Bailey, A., Allegrino, A., Wanzong, S., and Velden, C.: Introducing Atmospheric Motion Vectors Derived from the GOES-16 Advanced Baseline Imager (ABI). In 14th International Winds Workshop, Jeju City, South Korea, CIMSS. Available online at http://cimss.ssec.wisc.edu/iwwg/iww14/talks/01_Monday/1400_IWW14_ABI_AMVs_Daniels.pdf, 2018.

Formatted: Font: Times New Roman, Italic

Formatted: Font: Times New Roman

Formatted: Font: Times New Roman, Font color: Auto

Formatted: Font: Times New Roman

Formatted: Font: Times New Roman, Font color: Custom Color(RGB(34,34,34)),Pattern: Clear (White)

Formatted: Font: Times New Roman

de Kloe, J.: Aeolus L2B/L2C Product Handbook. Tech. rep., ESA, REF: AE-TN-KNMI-GS-0185, internal document available for registered Aeolus Cal/Val teams, 2019.

de Kloe, J., Stoffelen, A., Tan, D., Andersson, E., Rennie, M., Dabas, A., Poli, P., and Huber, D.: Aeolus Data Innovation Science Cluster DISC ADM-Aeolus Level-2B/2C Processor Input/Output Data Definitions Interface Control Document. Tech. rep., KMNI, Aeolus, DISC, REF: AED-SD-ECMWF-L2B-037. Available at: https://earth.esa.int/eogateway/documents/20142/37627/Aeolus-L2B-2C-Input-Output-DD-ICD.pdf, 2020.

~~Durre, I., Vose, R. S., and Wuertz, D. B.: Overview of the Integrated Global Radiosonde Archive. J. Climate, 19, 53-68, doi: https://doi.org/10.1175/JCLI3594.1, 2006.~~

European Space Agency (ESA): ADM-Aeolus Science Report, ESA SP-1311, 121 pp. Available at: https://earth.esa.int/documents/10174/1590943/AEOL002.pdf, 2008.

Garrett, K., Liu, H., Ide, K., Hoffman, R., and Lukens, K. E.: Optimization and Impact Assessment of Aeolus HLOS Wind Data Assimilation in NOAA's Global Forecast System. *Q. J. Roy. Meteor. Soc.*, in revision, 2022. [Manuscript QJ-21- 0307]

Grieger, J., Leckebusch, G. C., and Ulbrich, U.: Net Precipitation of Antarctica: Thermodynamical and Dynamical Parts of the Climate Change Signal. J. Climate, 29, 907-924, doi:10.1175/JCLI-D-14-00787.1, 2016.

Hoffman, R. N., Lukens, K. E., Ide, K., and Garrett, K.: A Collocation Study of Atmospheric Motion Vectors (AMVs) Compared to Aeolus Wind Profiles with a Feature Track Correction (FTC) Observation Operator. *Q. J. Roy. Meteor. Soc.*, ~~in review, 2021~~148, doi:10.1002/qj.4207, 2022.

Hoskins, B. J., and Hodges, K. I.: A new perspectives on Southern Hemisphere storm tracks. J. Climate, 18, 4108–4129, doi: https://doi.org/10.1175/JCLI3570.1, 2005.

Jung, J., Le Marshall, J., Daniels, J., and Riishojgaard, L. P.: Investigating height assignment type errors in the NCEP global forecasting system. In the 10th International Wind Workshop, Tokyo, Japan, EUMETSAT P.56. Available at: https://www-cdn.eumetsat.int/files/2020-04/pdf_conf_p56_s3_04_jung_v.pdf, 2010.

Key, J., Santek, D., and Dworak, R.: Polar winds from shortwave infrared cloud tracking. Proc. 13th Int. Winds Workshop, pp. 1-6, Monterey, California. Available online at: https://www.researchgate.net/profile/Jeffrey-Key-2/publication/309727571_Polar_winds_from_shortwave_infrared_cloud_tracking/links/581f84da08aea429b29907fd/Polar-winds-from-shortwave-infrared-cloud-tracking.pdf, 2016.

Le Marshall, J., Jung, J., Zapotocny, T., Redder, C., Dunn, M., Daniels, J., and Riishojgaard, L. P.: Impact of MODIS atmospheric motion vectors on a global NWP system. Aust. Met. Mag., 57, 45-51. Available at: http://citeseerx.ist.psu.edu/viewdoc/download?doi=10.1.1.222.6537&rep=rep1&type=pdf, 2008.

Formatted: Font: Times New Roman

Formatted: Font: Times New Roman, Italic

Formatted: Font: Times New Roman

Formatted: Font: Times New Roman, Italic

Formatted: Font: Times New Roman

Formatted: Font: Times New Roman

Formatted: Font: Times New Roman, Font color: Text 1

Liu, B., Guo, J., Gong, W., Zhang, Y., Shi, L., Ma, Y., Li, J., Guo, X., Stoffelen, A., de Leeuw, G., and Xu, X.: Intercomparison of wind observations from ESA's satellite mission Aeolus, ERA5 reanalysis and radiosonde over China. Atmos. Chem. Phys. Discuss., https://doi.org/10.5194/acp-2021-41, 2021.

Liu, H., Garrett, K., Ide, K., Hoffman, R. N., and Lukens, K. E.: A ~~Statistical~~Statistically Optimal Analysis of Systematic Differences ~~in Winds~~ between Aeolus ~~Level-2B Data~~ HLOS Winds and ~~the NOAA/FV3GFS. In preparation, 2021~~NOAA's Global Forecast System. *Atmos. Meas. Tech. Disc.*, submitted, https://doi.org/10.5194/amt-2022-20, 2022.

Martin, A., Weissmann, M., Reitebuch, O., Rennie, M., Geiß, A., and Cress, A.: Validation of Aeolus winds using radiosonde observations and numerical weather prediction model equivalents. Atmos. Meas. Tech., 14, 2167–2183, https://doi.org/10.5194/amt-14-2167-2021, 2021.

Nakamura, H., and Shimpo, A.: Seasonal Variations in the Southern Hemisphere Storm Tracks and Jet Streams as Revealed in a Reanalysis Dataset. J. Climate, 17, 1828-1844, doi: https://doi.org/10.1175/1520-0442(2004)017<1828:SVITSH>2.0.CO;2, 2004.

National Academies of Sciences, Engineering, and Medicine: Thriving on Our Changing Planet: A Decadal Strategy for Earth Observation from Space. National Academies Press, Washington, DC. doi:10.17226/24938, 2018.

Posselt, D., Wu, L., Mueller, K., Huang, L., Irion, F. W., Brown, S., Su, H., Santek, D., and Velden, C. S.: Quantitative Assessment of State-Dependent Atmospheric Motion Vector Uncertainties. J. Appl. Meteorol. Climatol., 58, 2479-2495, doi:10.1175/JAMC-D-19-0166.1, 2019.

Reitebuch, O., Lemmerz, C., Nagel, E., Paffrath, U., Durand, Y., Endemann, M., Fabre, F., and Chaloupy, M.: The Airborne Demonstrator for the Direct-Detection Doppler Wind Lidar ALADIN on ADM-Aeolus. Part I: Instrument Design and Comparison to Satellite Instrument, J. Atmos. Ocean. Tech., 26, 2501-2515, https://doi.org/10.1175/2009JTECHA1309.1, 2009.

Rennie, M., and Isaksen, L.: Guidance for Aeolus NWP impact experiments during the period September 2018 to November 2019. Tech. rep., ECMWF, Reading, United Kingdom, internal document available for registered Aeolus Cal/Val teams, 2019.

Rennie, M., and Isaksen, L.: The NWP impact of Aeolus Level-2B winds at ECMWF. Tech. rep., Aeolus Data Innovation Science Cluster DISC, Ref: AED-TN-ECMWF-NWP-025, doi: https://doi.org/10.21957/alift7mhr, 2020a.

Rennie, M., and Isaksen, L.: Assessment of the Impact of Aeolus Doppler Wind Lidar Observations for Use in Numerical Weather Prediction at ECMWF. In EGU 2020, Virtual. Available online at: https://presentations.copernicus.org/EGU2020/EGU2020-5340_presentation.pdf, 2020b.

Formatted: Font: Times New Roman
Formatted: Font: Times New Roman, Font color: Text 1
Formatted: Font: Times New Roman
Formatted: Font: Times New Roman, Font color: Text 1
Formatted: Font: Times New Roman, Pattern: Clear (Whit
Formatted: Font: Times New Roman, Pattern: Clear (Whit
Formatted: Font: Times New Roman, Pattern: Clear (Whit
Formatted: Font: Times New Roman, Pattern: Clear (Whit
Formatted: Font: Times New Roman

Rennie, M., Tan, D., Andersson, E., Poli, P., Dabas, A., de Kloe, J., and Stoffelen, A.: Aeolus Level-2B Algorithm Theoretical Basis Document: Mathematical Description of the Aeolus Level-2B Processor. Tech. rep., ESA, Version 3.4, Ref: AED-SD-ECMWF-L2B-038. Available at: https://earth.esa.int/eogateway/documents/20142/37627/Aeolus-L2B-Algorithm-ATBD.pdf, 2020.

Salonen, K., Cotton, J., Bormann, N., and Forsythe, M.: Characterizing AMV height-assignment error by comparing best-fit pressure statistics from the Met Office and ECMWF data assimilation systems. J. Appl. Meteor. Climatol., 54 (1), 225–242, doi:10.1175/JAMC-D-14-0025.1, 2015.

Santek, D., Dworak, R., Nebuda, S., Wanzong, S., Borde, R., Genkova, I., García-Pereda, J., Negri, R. G., Carranza, M., Nonaka, K., Shimoji, K., Oh, S. M., Lee, B.-I., Chung, S.-R., Daniels, J., and Bresky, W.: 2018 Atmospheric Motion Vector (AMV) Intercomparison Study. Remote Sens., 11, 2240, doi:10.3390/rs11192240, 2019.

Santek, D., García-Pereda, J., Velden, C., Genkova, I., Wanzong, S., Stettner, D., and Mindock, M.: 2014 AMV Intercomparison Study. In 12th International Winds Workshop, Copenhagen, Denmark, June 2014. Technical Report available online at: http://www.nwcsaf.org/aemetRest/downloadAttachment/225; Summary available online at: http://www.nwcsaf.org/aemetRest/downloadAttachment/226, 2014.

Santek, D., Hoover, B., Zhang, H., and Moeller, C.: Evaluation of Aeolus Winds by Comparing to AIRS 3D Winds, Rawinsondes, and Reanalysis Grids. In 15th International Winds Workshop, Virtual, 12-16 April 2021. Available online at https://www.ssec.wisc.edu/meetings/iwwg/2021-meeting/presentations/oral-santek/, 2021.

Schmetz, J., Holmlund, K., Hoffman, J., Strauss, B., Mason, B., Gaertner, V., Koch, A., and Van De Berg, L.: Operational cloud-motion winds from Meteosat infrared images. J. Appl. Meteor., 32, 1206–1225, doi: https://doi.org/10.1175/1520-0450(1993)032<1206:OCMWFM>2.0.CO;2, 1993.

Schmetz, J., Holmlund, K., Roesli, H. P., and Levizzani, V.: On the Use of Rapid Scans, Proceedings of the Fifth International Winds Workshop, Lorne, Australia, 28 February – 3 March 2000. EUM P28, Published by EUMETSAT, D-64295 Darmstadt, 227-234. Available online at http://cimss.ssec.wisc.edu/iwwg/iww5/S5-2_Schmetz-OnTheUse.pdf, 2000.

Stoffelen, A., Pailleux, J., Källén, E., Vaughan, J. M., Isaksen, L., Flamant, P., Wergen, W., Andersson, E., Schyberg, H., Culoma, A., Meynart, R., Endemann, M., and Ingmann, P.: The atmospheric dynamics mission for global wind field measurement. Bull. Amer. Meteor. Soc., 86 (1), 73–87, doi:10.1175/BAMS-86-1-73, 2005.

Straume, A. G., Elfving, A., Wernham, D., Kanitz, T., de Bruin, F., Buscaglione, F., von Bismarck, J., Lengert, W., and colleagues: Status of ESA's Doppler Wind Lidar Mission Aeolus. In 14th International Winds Workshop, Jeju City, South Korea, ESA. Available online at http://cimss.ssec.wisc.edu/iwwg/iww14/talks/04_Thursday/1000_IWW14_Aeolus_Straume.pdf, 2018.

Formatted: Font: Times New Roman

Straume, A. G., Parrinello, T., von Bismarck, J., Bley, S., Ehlers, F., and the Aeolus teams: ESA's Wind Lidar Mission Aeolus - status and scientific exploitation after 2.5 years in space. In 15th International Winds Workshop, Virtual, ESA. Available online at: https://www.ssec.wisc.edu/meetings/wp-content/uploads/sites/33/2021/02/IWW15_Presentation_AG_Straume.pdf, 2021.

Straume, A. G., Rennie, M., Isaksen, L., de Kloe, J., Marseille, G.-J., Stoffelen, A., Flament, T., Stieglitz, H., Dabas, A., Huber, D., Reitebuch, O., Lemmerz, C., Lux, O., Marksteiner, U., Weiler, F., Witschas, B., Meringer, M., Schmidt, K., Nikolaus, I., Geiss, A., Flamant, P., Kanitz, T., Wernham, D., von Bismarck, J., Bley, S., Fehr, T., Floberghagen, R., and Parinello, T.: ESA's space-based Doppler wind lidar mission Aeolus – first wind and aerosol product assessment results. EPJ Web Conferences, 237, 01007, https://do i.org/10.1051/epjconf/202023701007, 2020.

Straume-Lindner, A. G.: Aeolus Sensor and Product Description. Tech. rep., European Space Agency - European Space Research and Technology Centre, The Netherlands. REF: AE-SU-ESA-GS-000. Available at: https://earth.esa.int/eogateway/documents/20142/37627/Aeolus-Sensor-and-Product-Description.pdf, 2018.

Formatted: Font: Times New Roman

Trenberth, K.: Storm tracks in the Southern Hemisphere. J. Atmos. Sci., 48(19), 2159-2178, doi: https://doi.org/10.1175/1520-0469(1991)048<2159:STITSH>2.0.CO;2, 1991.

Velden, C. S., and Bedka, K. M.: Identifying the Uncertainty in Determining Satellite-Derived Atmospheric Motion Vector Height Attribution. J. Meteo. Clim., 48, 450-463, doi:10.1175/2008JAMC1957.1, 2009.

Velden, C., Daniels, J., Stettner, D., Santek, D., Key, J., Dunion, J., Holmlund, K., Dengel, G., Bresky, W., and Menzel, P.: Recent innovations in deriving tropospheric winds from meteorological satellites. Bull. Amer. Meteor. Soc., 86 (2), 205–223, doi:10.1175/BAMS-86-2-205, 2005.

Velden, C. S., Hayden, C. M., Nieman, S. J., Menzel, W. P., Wanzong, S., and Goerss, J. S.: Upper-tropospheric winds derived from geostationary satellite water vapor observations. Bull. Amer. Meteor. Soc., 78, 173–195, doi:10.1175/1520-0477(1997)078,0173:UTWDFG.2.0.CO;2, 1997.

Velden, C. S., and Holmlund, K.: Report from the working group on verification and quality indices (WG II). In 4th International Winds Workshop, Saanenmöser, Switzerland. Available online at https://cimss.ssec.wisc.edu/iwwg/iww4/p19-20_WGReport3.pdf, 1998.

von Bremen, L.: Using simulated satellite images to improve the characterization of Atmospheric Motion Vectors (AMVs) and their errors for Numerical Weather Prediction. NWP SAF, Version 1.4, REF: NWPSAF-EC-VS-015. Available at: http://research.metoffice.gov.uk/research/interproj/nwpsaf/vs.html, 2008.

Formatted: Font: Times New Roman

Weiler, F., Rennie, M., Kanitz, T., Isaksen, L., Checa, E., de Kloe, J., and Reitebuch, O.: Correction of wind bias for the lidar on-board Aeolus using telescope temperatures. ~~AMT, https://doi.org/10.5194/amt-2021-171,~~ Atmos. Meas. Tech., 14, 7167–7185, https://doi.org/10.5194/amt-14-7167-2021, 2021.

Wilks, D.: Statistical Methods in the Atmospheric Sciences, Volume 100, 3rd Edition. Academic Press, 9780123850225, 2011.

Wu, T.-C., Liu, H., Majumdar, S. J., Velden, C. S., and Anderson, J. L.: Influence of assimilating satellite-derived atmospheric motion vector observations on numerical analyses and forecasts of tropical cyclone track and intensity. Mon. Wea. Rev., 142, 49–71, doi:10.1175/MWR-D-13-00023.1, 2014.

Zuev, V. V., and Savelieva, E.: The cause of the spring strengthening of the Antarctic polar vortex. Dyn. Atmos. Oceans, 87, 101097, doi: 10.1016/j.dynatmoce.2019.101097, 2019.

Formatted: Font: Times New Roman, Font color: Black, Pattern: Clear (White)

Formatted: Font: Times New Roman, Font color: Black, Pattern: Clear (White)

Formatted: Font: Times New Roman, Font color: Black, Pattern: Clear (White)

Formatted: Font: Times New Roman, Font color: Text 1

Formatted: Font: Times New Roman

Formatted: Indent: Left: 0", Hanging: 0.5"